Published in final edited form as:
Am J Physiol Renal Physiol. 2006 May ; 290(5): F958–F974. doi:10.1152/ajprenal.00114.2005.

Functional MRI of the kidney: tools for translational studies of pathophysiology of renal disease

Pottumarthi V. Prasad
Evanston Northwestern Healthcare, Evanston, Illinois

Abstract

Magnetic resonance imaging (MRI) provides exquisite anatomic detail of various organs and is capable of providing additional functional information. This combination allows for comprehensive diagnostic evaluation of pathologies such as ischemic renal disease. Noninvasive MRI techniques could facilitate translation of many studies performed in controlled animal models using technologies that are invasive to humans. Such a translation is being recognized as essential because many proposed interventions and drugs that prove efficacious in animal models fail to do so in humans. In this article, we review the state-of-the-art functional MRI technique as applied to the kidneys.

Keywords

perfusion; renal function; blood oxygenation level-dependent; human; contrast agent

Over the last couple of decades, major progress in both in vivo and in vitro preparations and in invasive probe measurements of regional blood flow and oxygenation has led to many advances in the understanding of renal microcirculation and pathophysiology (2–4,12–14,23–25,29,38,49–52,77,78,102–106,125–127). Invasive probe technologies have allowed for very precise regional measurements of blood flow and tissue P_{O_2} that can be monitored over time and during pharmacological and/or physiological interventions. It is worth noting that these measurements are considered precise but not necessarily accurate, because, for example, Doppler flow probes do not measure regional flow in units of milliliters per minute per gram but rather provide relative measurements that can be used to follow changes in regional blood flow. Based on these types of measurements, roles of several endogenous factors in renal physiology and/or pathophysiology have been elucidated (e.g., prostaglandins, nitric oxide, etc.). Such understanding has produced novel hypotheses for intervention or preventive strategies. However, translation to humans has not always been successful (e.g., furosemide to prevent contrast nephropathy) (137). The availability of noninvasive methods would allow for better translation of findings from experimental models to humans.

Magnetic resonance imaging (MRI) is already well established as a diagnostic imaging modality providing exquisite soft tissue contrast and anatomic detail. Over the last two decades, tremendous advances have been made in terms of improved image quality and spatial coverage. Unlike other diagnostic imaging modalities, contrast in MRI can be modified in a variety of ways. This has led to efficient tissue characterization paradigms. In addition to the inherent contrast properties of MR, exogenous contrast can allow for further

Address for reprint requests and other correspondence: P. V. Prasad, Dept. of Radiology, Walgreen Jr. Bldg., Suite 507, Evanston Northwestern Healthcare, 2650 Ridge Ave., Evanston, IL 60201 (pprasad@enh.org).

refinements in tissue characterization. Many believe that the next revolution in MRI will be one of exogenous contrast agents [e.g., tissue-specific or targeted agents (131), smart contrast agents that are turned “on” only under specific conditions like the presence of a specific enzyme, etc. (82)]. MRI has a further advantage in that the methodology is equally applicable to small-animal models and hence allows for translation of results from preclinical to human applications.

In addition to anatomic and structural information, MRI provides unique opportunities to probe tissue “function” or “physiological status.” Function may mean different things for different types of tissues or organs. In functional brain MRI (fMRI), the term may refer to cognitive brain function. While the actual brain function occurs in neuronal activity, MRI is adept in characterizing the associated hemodynamic responses. Over the last decade, the field of fMRI has grown explosively and is fast becoming a regular feature in the news media. fMRI has diverse applications, such as probing human cognition (80,139), understanding how acupuncture may be beneficial (19,20), and serving as an expensive “lie” detector (53,64,81). Other organs and tissues within the body are also associated with specific functions and, while their evaluation may not be of interest to the lay audience, they may have significant implications in terms of understanding the physiology and pathophysiology of human disease. This review will elucidate such applications of MRI as applied to the kidney.

fMRI of tissue is motivated by the following: *1*) to better understand physiology and pathophysiology; *2*) to provide more comprehensive characterization of pathological lesions (e.g., clinical or functional significance of ischemic/stenotic lesions); and *3*) to provide either a more sensitive index or an early index of disease progression. An improved understanding of pathophysiology should allow for better design of interventions. Also, availability of fMRI techniques should allow for the evaluation of novel therapeutic interventions and preventive maneuvers. For these purposes, it may not be necessary for an fMRI technique to provide quantitative index of function, but the technique should be precise and sensitive to changes in function in response to pharmacological/physiological stimuli.

Before the discussion on specific fMRI methods can begin, it may be useful to review some basic principles of MRI and define some associated terminology.

PRINCIPLES OF MRI

Nuclei, notably hydrogen, that contain unpaired protons or neutrons are associated with a magnetic moment. In the presence of an external magnetic field, these magnetic moments (or spins) will precess about the field with the precessional frequency determined by the characteristic Larmor frequency ($\omega_L = \gamma B_0$; γ is the gyromagnetic ratio of the nucleus and B_0 is the applied magnetic field strength). The precession of the nuclear spin can be visualized as being similar to the wobbling of a spinning top in the presence of gravity before the top falls over. Hydrogen is the most important biological nucleus because of its abundance in the body in the form of water and lipids. The gyromagnetic ratio for ^{1}H is 42.57 MHz/T. Because the field strengths commonly used are in the range of a few Tesla, the Larmor frequency is on the order of megahertz, or in the radio frequency (RF) range. The net magnetic field experienced by the nucleus is a sum of the external field applied to the tissue and the much smaller fields generated by the electrons surrounding the nucleus. These additional fields alter the precession frequency of the nucleus by a tiny fraction known as the chemical shift. The value of the chemical shift is characteristic of the molecular group in which the nucleus resides and thus provides a distinctive signature for each metabolite. By analyzing the frequencies present in the MR signal, the investigator can identify the

metabolites in the tissue and estimate their concentration. This procedure forms the basis of magnetic resonance spectroscopy (MRS).

As the nucleus precesses about B_0, its magnetic moment rotates at the Larmor frequency ω_L, producing an oscillating magnetic field. The net magnetic field oscillations generated by all the nuclei in the sample can be detected with an RF receiver coil and constitute the MR signal. The signal will be zero, however, unless a sufficiently large number of the nuclei precess in synchrony. Resonant excitation using external RF energy can be used to establish such synchrony at least on a temporary basis and hence result in a detectable signal. Because the magnetic moments precess about the applied magnetic field, their individual magnetic moments can be expressed as longitudinal (along the applied field) and transverse (perpendicular to the applied field) components. At a state of equilibrium, the net transverse component is zero because of the random distribution of phase. However, because there are slightly more spins aligned toward than against the field, there is a net longitudinal component (can be termed polarization). The magnitude of this longitudinal component is determined by the field strength, and this is the reason higher field magnets result in higher signals. On excitation with RF energy precisely applied at the Larmor frequency and in the direction perpendicular to the applied magnetic field, the longitudinal component will be tipped to the transverse plane. This tipped magnetization (the sum of longitudinal components of all magnetic moments or spins) will be in synchrony, resulting in a detectable signal. The signal will not persist indefinitely, however, because of internuclear and intermolecular forces, which cause a loss of phase coherence among the spins and a corresponding attenuation of the transverse magnetization. The nuclei simultaneously lose energy to their surroundings, resulting in a recovery of the longitudinal magnetization to its equilibrium value. These processes are termed transverse (or T_2) and longitudinal (T_1) relaxation. Transverse (T_2) relaxation processes limit the available acquisition time (typically on the order of few ms) and broaden the spectroscopic line widths. However, because their rates depend on the molecular environment of the nuclei, they can be exploited to produce signal contrast among different tissues in MRI. Timing parameters such as echo time (TE; the time of data acquisition following the excitation pulse) and repetition time (TR; the time between the excitation pulses) are used to control the contrast properties based on T_2 and T_1, respectively.

Exogenous contrast agents usually enhance the relaxation rates and can be used to improve contrast on MR images. They can also be used as tracers to follow kinetics such as blood flow. Most approved contrast agents consist of gadolinium chelates (63). Gadolinium is paramagnetic and by binding to organic ligands, it is made biosafe. Such binding also results in slowing of the tumbling rate and hence the shortening of T_1 relaxation times. On the other hand, in the presence of magnetic field inhomogeneities the effective T_2 relaxation time becomes shorter and is termed T_2^*. Like many developments in MRI, T_2^* initially was seen as a problem, only to later become an effective method to enhance contrast (susceptibility-based contrast) and lead to many useful applications. They also form the basis of negative contrast agents such as iron oxide agents (11). Relaxivity of a contrast agent describes the change in relaxation rate per unit concentration of the agent, or in other words describes the potency of the agent.

To reconstruct an image or spatial distribution of ^1H nuclei, the signal from each point within the tissue must be correctly identified and mapped onto the corresponding point within the image. This is achieved with the use of magnetic field gradients, which alter the Larmor frequency of the nuclei in a spatially dependent manner. Combining these gradients with RF pulses of appropriate bandwidths results in the excitation of ^1H nuclei. Imaging can be performed using two-dimensional (2D) or 3D acquisitions, which involve the excitation of nuclei in a specified slice or slab of tissue, respectively. Once excited, all of the spins

within the slice or slab emit signals simultaneously. To produce images, it is necessary to identify the contribution from each point across the slice. This is achieved by encoding spatial information into the phase and frequency of the signal. Both slice-selective excitation and spatial encoding involve the use of magnetic field gradients along the three principal axes. Like digital pictures being described as a collection of pixels (picture elements), MR images are usually thought to be made of voxels (volume elements) determined by the combination of the spatial encoding gradients. The spatial selection process is usually assumed to be involved with static nuclei. However, if the volume of interest includes moving nuclei such as blood, some of the excited nuclei will be transported outside the selected volume. This forms the basis of arterial spin labeling (ASL), an effective method of measuring regional blood flow.

The most common field strength for clinical magnets is 1.5 T. However, 3.0 T is now commercially available and is FDA approved. Lower-field-strength magnets are available mostly for targeted applications such as extremity, open magnets for large or claustrophobic subjects, and interventional purposes, etc. For scanners used specifically for imaging small-animal models and ex vivo samples, higher field strengths are usually preferred to gain signal-to-noise ratio (SNR). These are typically between 4.7 and 14 T. Except for the field strength and the associated Larmor frequency, the rest of the principles remain the same. Because the net magnetization is determined by the field strength, the maximum SNR is limited by the field strength. One way to overcome this fundamental limitation is to polarize the spins by a nonmagnetic process. This is termed hyperpolarization and involves the use of lasers to create the spin polarization (7). Most of the work to date has been with hyperpolarized noble gases such as ^{129}Xe and ^{3}He. However, recent developments have shown the feasibility of ^{13}C in a water-soluble form (42,55).

A more extensive introduction to MRI principles is available elsewhere (Ref. 140 and references therein).

EVALUATION OF RENAL PHYSIOLOGICAL FUNCTION BY MRI

The most commonly used functional parameter is perfusion or regional blood flow expressed in milliliters of blood per second per 100 grams of tissue. MRI can provide quantitative, semiquantitative, or qualitative indexes that can be used to monitor changes in perfusion. For the kidney, the excretory function is an important physiological parameter. These two factors ultimately determine the P_{O_2} of renal tissue, which has been shown to be a critical factor in the pathophysiology of several renal diseases.

The following is an overview of the general principles involved in the evaluation of perfusion, renal excretory function, and intrarenal oxygenation using MRI. Illustrative examples are provided to highlight renal applications and/or their relevance to an understanding of the underlying renal physiology.

Perfusion

Blood perfusion is a crucial and fundamental physiological process that controls delivery of nutrients to tissue (33) and is therefore a parameter of critical interest in the assessment of tissue viability and function. Conventional in vivo perfusion measurements are based on the administration of exogenous tracers (62) detected by several different imaging techniques, such as X-ray computerized tomography (CT) (45) and positron emission tomography (PET) (40). These techniques are based on the indicator-dilution methods originally introduced a century ago by Stewart (138) and further developed by Zierler (153). In practice, this involves introduction of a known quantity of indicator into the system under study and

measurement of the concentration of the indicator as a function of time at one or more points downstream from the location of the injection.

There are number of nuclear magnetic resonance techniques for imaging and measuring tissue perfusion. Some are based on the indicator-dilution principle, and others depend on inherent MR mechanisms. Even though PET is still considered to be the gold standard for in vivo blood flow measurements, MR perfusion imaging is attractive because MR scanners are more readily available. Also, there is no ionizing radiation involved, and spatial resolution with MR is much superior to that obtained with PET. Furthermore, MRI offers the unique advantage of providing both anatomic and functional information with a single modality.

MR perfusion imaging techniques—In this section, we describe the basic mechanisms and derivation of perfusion information for several established MR perfusion techniques. The description is generally applicable to any tissue, and while many of the references provided in this section are concerned with brain perfusion, applications for the kidneys are also provided. It is useful to consider MR perfusion imaging techniques according to two major approaches: *1*) techniques based on administration of an exogenous contrast agent, and *2*) techniques that obviate the need for exogenous contrast administration. Each approach has advantages and disadvantages.

TECHNIQUES BASED ON EXOGENOUS CONTRAST AGENT ADMINISTRATION: In radionuclide imaging, the tissue concentration of a radioactive tracer is measured over time and, using suitable tracer kinetic models, several physiological parameters related to blood flow are estimated (66,153). In principle, a similar approach is possible with MRI if a suitable tracer is available and measurements can be made with sufficient temporal resolution. With the evolution of ultrafast MRI techniques (26,97), the possibility of monitoring exogenous tracer kinetics in vivo using MRI has become a reality, not only in the brain but in most organs in the body. Several gadolinium (Gd) chelates, such as Gd-diethylenetriamine pentaacetic acid (DTPA; Magnevist, Berlex Labs, Montville, NJ), Gd-HP-DO3A (Prohance, Bracco Diagnostics, Princeton, NJ), and Gd-DTPA-BMA (Omniscan, GE Healthcare, Milwaukee, WI) are being routinely used as contrast agents in MRI and can serve as tracers for blood flow measurements.

Because signal changes can be quantitatively related to changes in local concentration of Gd, tracer kinetic principles can be applied to relate the measured concentration-time curves to different physiological parameters. From the measurements of the tissue and arterial concentration curves [$C_{tissue}(t)$ and $C_{arterial}(t)$], the volume of distribution (V) of the agent can be calculated directly as

$$V = \frac{\int_0^\infty C_{tissue}(t)dt}{\int_0^\infty C_{arterial}(t)dt} \quad (1)$$

If the contrast material is restricted to the intravascular space, the volume of distribution reflects the blood volume V_b within the tissue. The arterial concentration-time curve can be measured using additional simultaneously acquired images that include the feeding artery (109). However, in the absence of arterial sampling, relative blood volumes can be inferred, assuming all the voxels within the image are fed by a single arterial source. It has been shown that with intravascular agents, accurate blood volume measurements can be obtained, but measurement of perfusion is more difficult (65). The central volume principle,

introduced by Stewart more than a century ago, relates the blood flow and blood volume to the mean transit time (τ) (138)

$$\tau = \frac{\text{regional blood volume(V)}}{\text{regional blood flow(F)}} \quad (2)$$

Mean transit time is usually estimated by calculating the first moment of the measured concentration-time curve as shown below

$$\frac{V}{F} = \frac{\int_0^\infty t C_{out}(t) dt}{\int_0^\infty C_{out}(t) dt} \quad (3)$$

where $c_{out}(t)$ is the concentration of the indicator measured at the outlet. This formulation, however, cannot be applied to imaging measurements because MR and other imaging measurements estimate the concentration within the tissue and not at the outlet (151). Flow measurements made using the above formulation, however, can yield a semiquantitative index that may be clinically useful (151). Equation 3 also assumes that $c_{out}(t)$ is measured in response to an instantaneous bolus of the tracer (mathematically described as a delta function). Because in practice this is not achievable, it is necessary to obtain an independent measure of the arterial concentration-time curve and deconvolve its distribution from the measured tissue concentration-time data.

There are currently no clinically approved MRI contrast agents that can be classified as intravascular. In all other tissue excluding the brain, Gd chelates leave the vascular space and distribute within the interstitial space. Hence, one cannot equate V to the blood volume. For the same reason, the signal intensity vs. time curve does not fully return to the baseline level over the measurement time. However, some useful perfusion indexes can be estimated and correlated with blood flow. Alternative pharmacokinetic models have been proposed to take into account the diffusion of contrast agents into the interstitium (62). These are being widely applied to functional evaluation of tumors because it is not just blood flow but also changes in “permeability” of vessels that are of interest. Dynamic (exogenous) contrast (agent)-enhanced MRI is widely being accepted as a mainstream clinical tool in oncology (101). Similar methods are being used in the evaluation of renal function because most of the currently approved Gd chelates for human use are freely filtered and excreted through the kidneys (54). These techniques can also be used to evaluate the excretory function.

Recent advances in MRI contrast agents have introduced so-called intravascular agents. Owing to their physical size or by attaching Gd to macromolecules, these agents remain within the vasculature for significantly long periods of time. While several agents have been proposed and shown to be efficacious in preclinical evaluation, few have progressed toward approval for clinical use. One such agent, MS-325 (EPIX Medical, Cambridge, MA), has completed phase III clinical trials (67). Ferumoxytol (Advanced Magnetics, Cambridge, MA) is an ultrasmall superparamagnetic iron oxide agent currently undergoing phase II clinical trials as a potential intravascular contrast agent (37,76).

TECHNIQUES BASED ON ENDOGENOUS CONTRAST MECHANISMS:

Techniques relying on exogenous contrast administration have certain limitations. Repeat studies are limited by the pharmacokinetics and the total amount of contrast that can be administered at one time. Perfusion MRI techniques that do not require exogenous contrast

agents are available. These are based on the inherent motion sensitivity of NMR (69,152), the use of erythrocytes as an endogenous contrast agent (taking advantage of the magnetic susceptibility effect of deoxyhemoglobin) (98–100), or water in the large vessels and subsequent utilization of it as a diffusible tracer (27,28). This last method allows for quantitative perfusion measurements. It is based on manipulating the magnetization of inflowing arterial blood and involves acquiring a flow-insensitive image and a flow-sensitive image and subtracting the former from the latter to remove the background tissue signals. For each image there is a delay period, during which the arterial blood enters the voxel in proportion to the perfusion *F* (Fig. 1). The techniques are, in general, called ASL methods.

Detailed quantitative models for the interpretation of flow effects have been developed by combining single-compartment kinetics with the Bloch equations for relaxation (154). However, the general quantitative features of inflow effects in these methods can be understood simply by considering the amount of blood entering the voxel and the magnetization carried by that blood. The equilibrium magnetization in the voxel is given by

$$M_0 = m_0 \mathrm{v} \mathrm{C_t} \tag{4}$$

where m_0 is the equilibrium magnetization of 1 mol of water, C_t is the concentration of water in tissue (mol/ml), and v is the volume of the voxel (ml). The magnetization within the voxel can be viewed as being influenced by two conflicting processes: magnetization delivered to the voxel by arterial flow and then lost by relaxation and by venous flow. Assuming water is nearly 100% extracted from the blood as it passes through the capillary bed, the rate of loss via venous flow is much less compared with that due to relaxation and thus can be neglected. The analysis can be simplified by assuming that the T_1 of blood and tissue are the same. With these definitions, we can derive approximate expressions for ΔM, the measured difference in magnetization.

The arterial magnetization per mole of water at time *t* after the inversion pulse (an RF pulse that tips the longitudinal magnetization by 180°) is m_0 for one image (without preinversion pulse) and $m_0[1 - 2e^{-t/\mathrm{T}_1}]$ for the other image, so $\Delta m = 2\, m_0 e^{-t/\mathrm{T}_1}$. Furthermore, the number of spins that entered the voxel up to time *t* after the inversion pulse is $N = F\mathrm{v}C_a t$. Then, the total magnetization difference is $\Delta M = N\, \Delta m$, or using the relationships defined above

$$\Delta M = 2M_0(\mathrm{F}/p)te^{-t/\mathrm{T}_1} \tag{5}$$

where the partition coefficient of water is $p = C_t/C_a$ (C_a is the concentration of arterial water). We can see that ΔM is proportional to FT, where F is the regional blood flow, and $\mathrm{T} = t\, \mathrm{e}^{-t/\mathrm{T}_1}$. The technique will be limited by T_1, and the magnitude of change is small (on the order of few %). Nevertheless, with state-of-the-art MRI systems, sufficiently high SNR can be achieved so that these small changes can be readily measured. In addition, the observed signal changes can be modeled directly in terms of *F*, thus providing the potential for obtaining quantitative measurement of perfusion.

Illustrative example: redistribution of intrarenal blood flow—Preliminary data were obtained in a small number of subjects ($n = 6$) undergoing extracorporeal shock wave lithotripsy (ESWL), which results in a physical shock to the renal parenchyma in the vicinity of the focal point (92). Figure 2 illustrates the signal intensity vs. time changes observed in

the renal parenchyma following the bolus injection of Gd-DTPA. Note the absence of corticomedullary differentiation on the flow-weighted images in the vicinity of the ESWL focal spot. Because Gd-DTPA is filtered through the kidneys without reabsorption, the signal intensity vs. time curves are in principle not amenable to analysis based on the central volume principle. However, semiquantitative indexes such as slope of the initial portion of the signal intensity vs. time curves can be used to compare data from two kidneys or from different subjects. Based on such analysis, cortical flow was reduced by ~ 29% with a concomitant increase in medullary blood flow by ~34% in the target region compared with the contralateral kidney. The redistribution of renal blood flow away from the cortex toward the medulla may be secondary to constriction of cortical arteries, resulting in shunting of blood to the medulla. This is known as Trueta phenomenon (146). Such shunting has been demonstrated in renal artery stenosis, sepsis, and trauma (88). Due to a lack of suitable techniques, the mechanisms responsible for such redistribution are not fully understood. It has been demonstrated that vasoactive substances may have an influence on the observed responses (141). In a subsequent study (17), it was shown that aminophylline abolished the drop in cortical flow with no significant change in the medulla. These results are consistent with previous findings that adenosine antagonism may prevent decline of renal function (10,36).

Even with extracellular agents, it has been shown that, by combining the upslope measurements with signal intensity vs. time data from the arterial blood supply, it is possible to derive quantitative absolute blood flow measurements (148). This model assumes that, before exiting the kidney, the contrast agent behaves similarly to microspheres. Accordingly, renal perfusion per unit volume can be estimated by the following formula

$$\frac{\mathrm{RP}}{\mathrm{Volume}} = \frac{\max\ \mathrm{slope}_{\mathrm{renal}}}{\max \Delta\left(\frac{1}{T_1}\right)_{\mathrm{arterial}}} \tag{6}$$

The slope refers to the leading edge of the first pass signal intensity vs. time curve, and RP is renal perfusion. The denominator refers to the peak change in T_1 relaxation rate in the arterial blood. This measurement has been validated in an animal model in a recent study (89).

Illustrative example: intravascular agents for renal perfusion MRI—

Alternatively, with the use of novel intravascular contrast agents, quantitative perfusion indexes can be obtained using the central volume principle. This was demonstrated using MS-325, the first small-molecule blood-pool contrast agent for MRI (67). This Gd chelate binds reversibly with serum protein in plasma and leads to high relaxivity (5–10 times that of Gd-DTPA over a range of magnetic field strengths and concentrations). Excretion is still efficient because the protein binding is reversible. Due to these properties, MS-325 provides strong, persistent enhancement of the vascular space on T_1-weighted MR images. Using this agent, first-pass perfusion MRI was used in an animal model of chronic renal artery stenosis to demonstrate feasibility of quantitative regional blood flow measurements (110).

Figure 3 is an example of first-pass perfusion MRI using a novel iron oxide-based contrast agent, ferumoxytol. Ferumoxytol, currently undergoing phase II clinical trials (37,76), consists of nanoparticles of iron oxide with a dextran coating for biocompatibility. Shown are T_2*-weighted images of a kidney obtained following a bolus administration of ferumoxytol (1 mg/kg) in an anesthetized rabbit. Using a similar agent, quantitative regional blood flow estimations were reported (8,132) using the central volume principle.

Illustrative example: ASL for renal perfusion MRI—ASL has been used for evaluation of renal perfusion (18,28,61,85,87,115,150). The combination of MR angiography and ASL perfusion imaging provides a comprehensive assessment of both renovascular and renoparenchymal disease and hence provides a noninvasive approach to differentiate between diseased and normal kidneys (87). These techniques may be particularly attractive for repeat measurements to monitor pharmacological and/or physiological stimuli. While ASL techniques provide adequate sensitivity to evaluate cortical flow, they may not be suitable for the evaluation of medullary blood flow. This may be related to relatively low blood flow to the region and also to the increased transit time for the labeled blood to arrive at the medulla.

Current status of perfusion MRI for routine clinical use—While proof of principle confirmations have been made with several methods of renal perfusion MRI, these techniques have not been translated into clinical practice. Myocardial perfusion, in clinical use in most major academic centers today, required more than a decade since the initial studies were performed. First-pass contrast-enhanced perfusion MRI in the brain is more widely used in the clinic; however, there is still no consensus on processing and presentation of the data.

The impact of perfusion MRI in the evaluation of ischemic renal diseases such as renal artery stenosis will depend on a better understanding of the relationship between the bulk flow in a stenosed vessel and perfusion within the kidney, as well as the compensatory mechanisms that may preserve tissue perfusion. In ischemic heart disease, while coronary artery stenosis is detected with angiography, its functional significance is evaluated by myocardial perfusion, particularly with a combination of “stress” (108). In ischemic brain injury, such as during a stroke, angiography is primarily used to detect stenosis in major vessels and perfusion to evaluate regional blood flow deficits (5). However, in the kidney, the status quo is to detect renal artery stenosis by angiography (including MR angiography) and radionuclide renography, particularly in combination with angiotensin-converting enzyme (ACE) inhibition (144). Blood flow measurements in the renal arteries [by Doppler ultrasound (118) and MRI (133,134)] are being evaluated as a means to assess functional significance. Preliminary experience with perfusion MRI measurements in a chronic stenosis model using two different techniques (110,115) has not yet yielded consistent results. Physiological adaptation may explain the inconsistency. “Stress” perfusion imaging paradigms may need to be considered. In addition to the diagnostic application of perfusion MRI, there is also the potential value of noninvasive perfusion information with adequate spatial resolution to resolve the intrarenal compartments to better understand renal physiology in both health and disease.

Renal Excretory Function by Dynamic Contrast Enhancement Techniques

Like inulin and iodinated contrast agents, Gd chelates are predominantly cleared by glomerular filtration (98%) without tubular secretion or reabsorption. Therefore, calculation of glomerular filtration rate (GFR) is feasible using Gd-DTPA by the formula

$$GFR = U * V / P \tag{7}$$

where V is the urine flow rate (ml/min), U is the substance concentration in urine, and P is the substance concentration in plasma.

With MR, the measurement of concentration of the contrast agent is based on relaxivity changes in urine, blood, or kidney or via measurement of signal intensity within the kidneys.

One of the first studies to show the feasibility of GFR measurements by MR was based on blood and urine samples and ex vivo MR measurements of T_1 (21). A very good correlation was demonstrated with radionuclide-based GFR measurement. Subsequently, in vivo measurements of Gd concentrations in the blood were used to estimate GFR. In this method, the extraction fraction (EF) was estimated by measuring the difference in Gd concentration ([Gd]) in the artery and vein.

$$EF_{Gd} = \frac{[Gd]_{artery} - [Gd]_{vein}}{[Gd]_{artery}} \tag{8}$$

Gd concentration was estimated using T_1 measurements before and after contrast administration in the renal artery and vein. With an additional measurement of renal blood flow (RBF) using the phase-contrast method in the renal artery, GFR can be estimated using

$$GFR = EF_{Gd} * RBF * (1 - Hct) \tag{9}$$

where Hct refers to the hematocrit. Several groups have published results based on this approach to measure single-kidney GFR (22,31,96). The major disadvantage of this approach is the necessity for concentration and blood flow measurements in relatively small vessels.

Alternately, single-kidney GFR can be estimated based on monitoring intrarenal signal kinetics. Bauman and Rudin (9) proposed a first-order kinetic model of the kidney that consists of two compartments, the cortex and medulla, and a rate constant between the two representing the rate of clearance of tracer from the cortex.

$$\frac{d[Gd]_m}{dt} = k * [Gd]_c \tag{10}$$

$[Gd]_{m,\,c}$ are the time-varying concentrations of Gd in the medulla and cortex, respectively, and k is the flow rate between the two compartments, presumed to represent renal clearance. Preliminary validation in a small-animal model has been reported (68). An alternate two-compartment model (136) and a more expansive multicompartmental model have also been proposed (70). An alternative analytic method based on the Patlak plot technique has also been proposed, and preliminary validation has been provided (47,48). This method also assumes a two-compartment model; however, these include vascular and nephron compartments. The renal tissue concentration of Gd is presumed to be the sum of the vascular and nephron compartments. Therefore, the concentration of Gd in one kidney [$K(t)$] is given by

$$K(t) = B(t) + Q(t) \tag{11}$$

where B and Q refer to the vascular and nephron compartments. If Gd concentration in the vascular compartment is assumed to be the same as that in the descending aorta

$$B(t)=c_1 b(t) \tag{12}$$

where b is the concentration of Gd in the aorta and c_1 is the vascular volume fraction within the kidney. The concentration of Gd in the nephron is proportional to the integral of the concentration within the vascular compartment as per the usual definition of clearance. Thus

$$Q(t)=c_2 \int_0^{t_1} b(t)dt \tag{13}$$

where c_2 represents the clearance of Gd from the vascular to nephron compartment. Substituting for B and Q in to Eq. 11 and rearranging terms

$$\frac{K(t_1)}{b(t_1)}=c_1+c_2\frac{\int_0^{t_1} b(t)dt}{b(t_1)} \tag{14}$$

This is now in the form of a linear equation with the slope representing the clearance (which within certain limits can be assumed to represent GFR), and the intercept a measure of vascular volume. Corrections for hematocrit and relaxivity differences can be incorporated. Overall, the advantage of this technique is its relative simplicity in terms of analysis, an important consideration for routine clinical use. This method is currently being evaluated in a clinical setting (58).

Other applications in which dynamic contrast enhancement kinetics could provide valuable information for comprehensive evaluation include ureteral obstruction (59,93,123,124) and evaluation of renal transplants (1,30).

Current status of GFR estimation by MRI for routine clinical use—As with perfusion MRI, proof-of-concept validations have been reported with many different approaches. However, the techniques are still evolving and have not been translated in to the clinic. Like perfusion MRI, acquisition of dynamic contrast-enhanced data is relatively straightforward. It is the analysis of the acquired data that is not yet streamlined. If analysis tools were available on the scanner or associated platforms, this could increase the clinical availability. Qualitative or semiquantitative approaches can be readily implemented in the clinic (as illustrated in the example below).

Illustrative example: functional significance of renal artery stenosis—Most anatomic tests, such as conventional angiography and MR and CT angiography, are limited in their ability to diagnose renal vascular disease because they rely on renal artery stenosis as the sole criterion. A physiological imaging diagnosis of renal artery stenosis is currently made using angiotensin-converting enzyme inhibitor (ACE-I) renal scintigraphy and is arguably a good predictor of response to therapy (16,39). The signal intensity-time curves obtained with predominantly T_1-weighted sequences (such as those used for acquiring contrast-enhanced MR angiography) can be used in concert with ACE inhibition to differentiate kidneys supplied by stenotic renal arteries (44,114). This approach parallels ACE-I renal scintigraphy, and hence is called MR-renography. The advantage of MRI is that it can be readily combined with anatomic information such as MR angiography. Preliminary feasibility has been reported both in animal models (Fig. 4) (114) and in human subjects (44).

These data could be subject to semiquantitative analysis to compute split renal function. By integrating the signal intensity measured over the renal parenchyma (usually between 1 and 2 min after injection of contrast) and multiplying by the volume of the region of interest, one can estimate the single-kidney function (F_{left} and F_{right}). Split renal function is given by

$$F\% = \frac{F_{left}}{(F_{left} + F_{right})} \quad (15)$$

A high correlation ($r = 0.97$, $P < 0.001$) was reported for F% estimates by MR renography compared with radionuclide renography (145).

Given the importance of renal artery stenosis in the diagnosis of renal vascular disease, it is important to consider other techniques with potential predictive value. MR is capable of estimating blood flow velocities as a function of cardiac phase (cine phase-contrast-flow measurements), and hence measurements of resistive index [1 − (end-diastolic velocity/maximal systolic velocity) × 100] are potentially feasible. Schoenberg et al. (134) have reported on a multireader tricenter study to evaluate efficacy of MR angiography and cine-PC-flow measurements in characterizing renal artery stenosis. The combined techniques led to better interobserver agreement. Even though potentially feasible, the resistive index was not estimated in this study. A further study reported that the combination of cine PC flow and MR perfusion measurements by ASL technique offers a comprehensive assessment of both renovascular and renoparenchymal disease and provides a noninvasive approach to differentiating between these kidneys and normal kidneys (87). These studies highlight the notion of comprehensive evaluation afforded by MRI methods. However, these studies only provide proof-of-principle, and further studies based on multicenter and multivendor platforms are necessary for widespread acceptance.

Oxygenation

Oxygen is one of the key nutrients transported by blood to the tissue, and in most tissues regional P_{O_2} closely follows the level of regional blood flow. Although total renal blood flow is the highest in the body with respect to organ weight, most of it is directed toward the cortex to optimize glomerular filtration and reabsorption of solute. By contrast, blood flow to the medulla is low, to preserve osmotic gradients and enhance urinary concentration (15). Furthermore, the anatomic arrangement of the tubules and the vasa recta within the medulla leads to diffusion of oxygen from the arterial to the venous side. The medullary thick ascending limb is primarily responsible for the generation of an osmotic gradient by active reabsorption of sodium, a process that requires a large amount of oxygen. Taken together, the medulla functions in a hypoxic milieu (15,34).

Blood oxygenation level-dependent MRI for study of renal medullary hypoxia

—Blood oxygenation level-dependent (BOLD) MRI has been used extensively in other organs (e.g., the brain) (86,120,147). The BOLD MRI technique exploits the fact that the magnetic properties of hemoglobin vary, depending on whether it is in the oxygenated or deoxygenated form. This affects the T_2* relaxation time of the neighboring water molecules and, in turn, influences the MRI signal on T_2*-weighted images. The rate of spin dephasing, R_2* (=1/T_2*), is closely related to the tissue content of deoxyhemoglobin. Because the P_{O_2} of capillary blood is assumed to be in equilibrium with the surrounding tissue, changes estimated by BOLD MRI can be interpreted as changes in tissue P_{O_2} (32,95,111,112). A strong correspondence has been demonstrated between renal BOLD MRI measurements in humans (111,112) and rodents (117) and earlier animal data obtained using invasive microelectrodes (12). Changes in medullary P_{O_2} are produced by the administration of

furosemide, but not acetazolamide. Furosemide, a loop diuretic, reduces the reabsorptive work in the thick ascending limbs and hence improves medullary oxygenation, whereas acetazolamide results in similar diuretic effect but acts on the cortical portion of the nephron and shows minimal change in medullary oxygenation. While Brezis et al. (12) reported an increase in cortical P_{O_2} following acetazolamide using microelectrodes, BOLD MRI failed to record a similar response, probably due to the reduced sensitivity to cortical P_{O_2} based on the hemoglobin oxygen saturation curve. Figure 5 illustrates BOLD MRI application to intrarenal oxygenation, from a 24-g mouse to a 250-g rat, all the way to a 70-kg human.

BOLD MRI: application to ischemic renal injury—Early studies tested the hypothesis that the compromise of endogenous protective mechanisms fails to maintain medullary oxygenation status and leads to manifestation of disease and/or disease progression. Using the BOLD MRI technique, it was shown that age and diabetes, both recognized as predisposing factors for acute renal failure, are associated with reduced prostaglandin production, a hypothesized protective mechanism (35,113). This was done by demonstrating differences in the response to water loading compared with age-matched controls. Furthermore, it was demonstrated that young subjects, who showed a significant improvement in renal medullary P_{O_2} during water loading, failed to do so when pretreated with ibuprofen. Prior observations using microelectrodes suggest that the development of radiocontrast nephropathy requires elimination of prostaglandin and nitric oxide systems (4). These observations were duplicated using BOLD MRI (116).

Other applications of BOLD MRI measurements include studying effects of renal artery stenosis (60) and diabetes (121). In a carefully performed study in large animals, Juillard et al. (60) found significantly reduced oxygenation in both the cortex and medulla during acute reduction in blood flow. The authors also comment that “BOLD MRI is the only technique currently available that allows noninvasive measurement of oxygen content in the kidney.” They also suggest that new functional tools, such as BOLD, capable of detecting ischemia and characterizing patterns of intrarenal oxygen levels, may assist in identifying patients that may more likely benefit from therapeutic interventions. Alford et al. (6) also used an acute renal artery obstruction model and observed a significant increase in renal R_2* values. The contralateral kidney showed no such change. They also demonstrated the R_2* values return to baseline on release of the obstruction.

In swine, Pedersen et al. (107) have shown correspondence between BOLD MRI and simultaneous microelectrode measurements performed within the contralateral kidney. They also demonstrated changes in intrarenal oxygenation following 24-h unilateral ureteral obstruction (UUO). They observed the cortical R_2* to increase (implying lower oxygenation) while the medullary R_2* values decreased (implying better oxygenation). The mechanisms involved are not yet understood, however, metabolic work in the medulla may be reduced during unilateral ureteral obstruction.

In probably the first preliminary clinical application of the BOLD MRI technique, Sadowski et al. (128) have shown that medullary R_2* values are significantly lower in transplanted kidneys that were in acute rejection compared with functional transplants and transplants with acute tubular necrosis (ATN). This finding is important because it could potentially minimize the use of percutaneous transplant biopsies.

Ries et al. (121) have used a model for type I diabetes, streptozotocin (STZ)-induced diabetes in rats, and have shown using BOLD MRI that the oxygenation in all compartments of the kidney is significantly reduced. By comparing the observed changes on BOLD with histological changes, the authors further conclude that the observed MR changes are not

influenced by anatomic or histological changes. The observed change is interpreted as due to increased oxygen consumption related to hyperfiltration.

BOLD MRI: application to hypertension—Renal dysfunction may also play a role in the development of hypertension in humans and laboratory animals (56,57). A role for the kidney was first proposed three decades ago (46), based on evidence that renal function vs. blood pressure curve shifts to the right in kidneys with hypertension.

BOLD MRI studies indicate that kidneys of hypertensive rats have reduced nitric oxide bioavailability (74) that may be reversed by suitable pharmacological interventions such as superoxide scavengers (73). Baseline R_2* values in the renal medulla of spontaneously hypertensive rats were significantly high (i.e., low oxygenation) compared with those in the Wistar-Kyoto strain and do not respond to nitric oxide synthase inhibition by N^{ω}-nitro-L-arginine methyl ester (Fig. 6*A*). Similarly, it was also shown that renal medullary R_2* drops (i.e., oxygenation improves) significantly following administration of tempol in spontaneously hypertensive rats but not in Wistar-Kyoto rats (Fig. 6*B*). With a better understanding of these and other such protective mechanisms, it may be possible to implement suitable interventions to prevent renal disease progression associated with hypertension. More importantly, these measurements may be extended to human studies (71,72).

Current status of renal BOLD MRI for routine clinical use—Compared with perfusion imaging and renography, BOLD MRI is a relatively simple implementation. Even though the multiple-gradient echo (mGRE) sequence is not yet a standard sequence, it is available as a research sequence on most major vendor platforms. The analysis is relatively simple and could be performed on scanner platforms. Both short (155)- and long-term (75) reproducibility have been established. As more investigators become interested in performing these studies, the number of applications will increase.

Other fMRI Techniques and Recent Developments

We have covered three major fMRI methods that are relatively mature and could allow for translation to human studies today. However, there are several other techniques that have been demonstrated as potential fMRI methods with specific applications to the kidney. These include diffusion measurements in the kidney (79,94,122,135), pH measurements (119), and, more recently, sodium MRI (84). While diffusion measurements certainly provide opportunities for tissue characterization, it is not quite clear what the measured values represent in terms of the functional status of the kidney. A more recent development is the feasibility of performing sodium (Na) MRI (84) to follow the urinary concentrating process directly. MRI has the ability to directly measure the tissue sodium concentration noninvasively. However, it necessitates custom coils that either are tuned to Na frequency or doubly tuned coils so that one can perform both proton (H) and Na MRI. Because Na MRI is at least an order of magnitude lower compared with proton MRI and the concentration of Na is 100-fold less than water, the signal-to-noise ratios are significantly lower on Na MRI compared with proton images.

There are a number of other developments that may potentially open up new methods to probe tissue characterization and function by MRI. These include novel contrast agents that allow for evaluation of regional pH (119) and hyperpolarized ^{13}C (42), which may give rise to novel applications for both imaging and spectroscopic applications.

Pathologically altered renal physiology can manifest as perturbations in both systemic and renal pH. Methodologies to image the spatial distribution of tissue pH would have considerable biomedical and clinical relevance by enabling noninvasive assessment of

disease extent, progression, and response to therapy. Several approaches have been proposed to measure tissue pH by magnetic resonance. Some exploit the difference in ^{31}P or ^{1}H resonances (90,142,149). However, these are limited in terms of imaging applications. Certain Gd complexes (e.g., Gd-DOTA-4AMP, Macrocyclics, Dallas, TX) offer the possibility of imaging pH with a spatial resolution comparable to standard MRI (90,142,149). Whereas proof-of-concept has been demonstrated (119), the technique is in the very early stages of development and several practical issues must be addressed, including the applicability of the compounds to human use.

Conventional polarization (as defined earlier) is limited by field strength. However, there are alternate methods to improve the polarization of exogenous substances and hence are termed hyperpolarization. Hyperpolarized noble gases (^{3}He and ^{129}Xe) are being successfully used for MRI of airways in the lungs (83,129,130). However, the low solubility of these gases in blood makes these agents unsuitable for most other applications. The feasibility of hyperpolarizing ^{13}C as a part of a water-soluble molecule has been demonstrated. Two polarization techniques, parahydrogen-induced polarization (43) and dynamic nuclear polarization (42) have been shown to be useful in producing hyperpolarized ^{13}C. High polarizations on the order of 15% are possible with a concentration of 200 mM in water. These properties make it very promising for MR angiography and such feasibility was recently demonstrated (143). Preliminary demonstration of cerebral perfusion has also been reported (55). The major advantage of using hyperpolarized ^{13}C for perfusion imaging is that the signal is directly related to concentration of the agent, a serious issue with currently available dynamic susceptibility-based contrast approaches. However, other issues arise with the use of hyperpolarization. Higher concentrations and longer relaxation times of the agent may be necessary for blood flow measurements (55). Also, one has to measure the depolarization rate to allow for quantitative blood volume and mean transit time estimates.

The concept can be further developed to produce hyperpolarized ^{13}C in endogenous substances. Feasibility has been demonstrated in angiograms using [^{13}C]urea polarized by the dynamic nuclear polarization method. This could potentially lead to functional/molecular imaging using endogenous substances (41), because MRI of ^{13}C-labeled glucose was shown to be feasible years ago (91). By hyperpolarization, these techniques could be made more efficacious for routine applications. This approach will combine the superior spatial resolution of MRI and the specificity of techniques like PET. The major limitation of this technology is that the polarization is relatively short lived, on the order of 1 min. This will necessitate fast imaging approaches and also the need for an onsite drug delivery system.

CONCLUDING REMARKS

We have reviewed the current state-of-the-art techniques in terms of fMRI as applied to the kidneys. While the motivation for fMRI is multifold, we believe the utility for translational research from preclinical models to humans is most compelling. The particular advantages of MRI technology are *1*) it is scalable from mouse to humans; and *2*) its noninvasive nature make it useful for longitudinal studies.

Because exquisite anatomic detail can be obtained, fMRI is uniquely suitable for a better understanding of spatial and temporal responses to interventions.

The ability to perform multiple fMRI techniques could allow for multiparametric analysis; e.g., perfusion and BOLD MRI could potentially allow for the separation of blood flow changes from oxygenation changes or Na and BOLD MRI to monitor in parallel the Na excretion dynamics along with intrarenal oxygenation changes.

Because access to MRI until recently has been predominantly in the radiological community, the applications have been primarily driven by diagnostic utility and specific research questions. However, as MRI is gaining widespread acceptance as a functional or physiological imaging tool and with more cross-disciplinary collaborations being established, its role in understanding physiology and pathophysiology will increase. This may result in improved sensitivity and/or specificity of diagnostic evaluations, and more importantly, identification of biomarkers to evaluate novel therapeutic and preventive maneuvers.

Acknowledgments

The images in Fig. 5B (unpublished) were obtained in collaboration with Dr. David Basile.

GRANTS

This work was supported in part by National Institute of Diabetes and Digestive and Kidney Diseases Grant DK-53221.

References

1. Agildere AM, Tarhan NC, Bozdagi G, Demirag A, Niron EA, Haberal M. Correlation of quantitative dynamic magnetic resonance imaging findings with pathology results in renal transplants: a preliminary report. Transplant Proc. 1999; 31:3312–3316. [PubMed: 10616489]
2. Agmon Y, Brezis M. Effects of nonsteroidal anti-inflammatory drugs upon intrarenal blood flow: selective medullary hypoperfusion. Exp Nephrol. 1993; 1:357–363. [PubMed: 8081987]
3. Agmon Y, Dinour D, Brezis M. Disparate effects of adenosine A_1- and A_2-receptor agonists on intrarenal blood flow. Am J Physiol Renal Fluid Electrolyte Physiol. 1993; 265:F802–F806.
4. Agmon Y, Peleg H, Greenfeld Z, Rosen S, Brezis M. Nitric oxide and prostanoids protect the renal outer medulla from radiocontrast toxicity in the rat. J Clin Invest. 1994; 94:1069–1075. [PubMed: 8083347]
5. Ahmed M, Masaryk TJ. Imaging of acute stroke: state of the art. Semin Vasc Surg. 2004; 17:181–205. [PubMed: 15185185]
6. Alford SK, Sadowski EA, Unal O, Polzin JA, Consigny DW, Korosec FR, Grist TM. Detection of acute renal ischemia in swine using blood oxygen level-dependent magnetic resonance imaging. J Magn Reson Imaging. 2005; 22:347–353. [PubMed: 16104014]
7. Appelt S, Ben-Amar Baranga A, Erickson CJ, Romalis MV, Young AR, Happer W. Theory of spin-exchange optical pumping of ^{3}He and ^{129}Xe. Physiol Rev. 1998; 58:1412–1439.
8. Aumann S, Schoenberg SO, Just A, Briley-Saebo K, Bjornerud A, Bock M, Brix G. Quantification of renal perfusion using an intravascular contrast agent (part 1): results in a canine model. Magn Reson Med. 2003; 49:276–287. [PubMed: 12541248]
9. Baumann D, Rudin M. Quantitative assessment of rat kidney function by measuring the clearance of the contrast agent Gd(DOTA) using dynamic MRI. Magn Reson Imaging. 2000; 18:587–595. [PubMed: 10913720]
10. Bidani AK, Churchill PC. Aminophylline ameliorates glycerol-induced acute renal failure in rats. Can J Physiol Pharmacol. 1983; 61:567–571. [PubMed: 6883209]
11. Bjornerud A, Johansson L. The utility of superparamagnetic contrast agents in MRI: theoretical consideration and applications in the cardiovascular system. NMR Biomed. 2004; 17:465–477. [PubMed: 15526351]
12. Brezis M, Agmon Y, Epstein FH. Determinants of intrarenal oxygenation. I. Effects of diuretics. Am J Physiol Renal Fluid Electrolyte Physiol. 1994; 267:F1059–F1062.
13. Brezis M, Heyman SN, Dinour D, Epstein FH, Rosen S. Role of nitric oxide in renal medullary oxygenation. Studies in isolated and intact rat kidneys. J Clin Invest. 1991; 88:390–395. [PubMed: 1864953]
14. Brezis M, Heyman SN, Epstein FH. Determinants of intrarenal oxygenation. II. Hemodynamic effects. Am J Physiol Renal Fluid Electrolyte Physiol. 1994; 267:F1063–F1068.

15. Brezis M, Rosen S. Hypoxia of the renal medulla—its implications for disease. N Engl J Med. 1995; 332:647–655. [PubMed: 7845430]
16. Canzanello VJ, Textor SC. Noninvasive diagnosis of renovascular disease. Mayo Clin Proc. 1994; 69:1172–1181. [PubMed: 7967780]
17. Chan AJ, Prasad PV, Priatna A, Mostafavai MR, Sunduram C, Saltzman B. Protective effect of aminophylline on renal perfusion changes induced by high-energy shockwaves identified by Gd-DTPA-enhanced first-pass perfusion MRI. J Endourol. 2000; 14:117–121. [PubMed: 10772502]
18. Chen Q, Siewert B, Bly BM, Warach S, Edelman RR. STAR-HASTE: perfusion imaging without magnetic susceptibility artifact. Magn Reson Med. 1997; 38:404–408. [PubMed: 9339441]
19. Cho ZH, Chung SC, Jones JP, Park JB, Park HJ, Lee HJ, Wong EK, Min BI. New findings of the correlation between acupoints and corresponding brain cortices using functional MRI. Proc Natl Acad Sci USA. 1998; 95:2670–2673. [PubMed: 9482945]
20. Cho ZH, Oleson TD, Alimi D, Niemtzow RC. Acupuncture: the search for biologic evidence with functional magnetic resonance imaging and positron emission tomography techniques. J Altern Complement Med. 2002; 8:399–401. [PubMed: 12230898]
21. Choyke PL, Austin HA, Frank JA, Girton ME, Diggs RL, Dwyer AJ, Miller L, Nussenblatt R, McFarland H, Simon T. Hydrated clearance of gadolinium-DTPA as a measurement of glomerular filtration rate. Kidney Int. 1992; 41:1595–1598. [PubMed: 1501414]
22. Coulam CH, Lee JH, Wedding KL, Spielman DM, Pelc NJ, Kee ST, Hill BB, Bouley DM, Derby GC, Myers BD, Sawyer-Glover AM, Sommer FG. Noninvasive measurement of extraction fraction and single-kidney glomerular filtration rate with MR imaging in swine with surgically created renal arterial stenoses. Radiology. 2002; 223:76–82. [PubMed: 11930050]
23. Cowley AW Jr. Control of the renal medullary circulation by vasopressin V1 and V2 receptors in the rat. Exp Physiol. 2000; 85:223S–231S. [PubMed: 10795926]
24. Cowley AW Jr, Mattson DL, Lu S, Roman RJ. The renal medulla and hypertension. Hypertension. 1995; 25:663–673. [PubMed: 7721413]
25. Cowley AW, Roman RJ, Fenoy FJ, Mattson DL. Effect of renal medullary circulation on arterial pressure. J Hypertens Suppl. 1992; 10:S187–193. [PubMed: 1291653]
26. Davis CP, McKinnon GC, Debatin JF, von Schulthess GK. Ultra-high-speed MR imaging. Eur Radiol. 1996; 6:297–311. [PubMed: 8797999]
27. Detre JA, Leigh JS, Williams DS, Koretsky AP. Perfusion imaging. Magn Reson Med. 1992; 23:37–45. [PubMed: 1734182]
28. Detre JA, Zhang W, Roberts DA, Silva AC, Williams DS, Grandis DJ, Koretsky AP, Leigh JS. Tissue specific perfusion imaging using arterial spin labeling. NMR Biomed. 1994; 7:75–82. [PubMed: 8068529]
29. Dinour D, Brezis M. Effects of adenosine on intrarenal oxygenation. Am J Physiol Renal Fluid Electrolyte Physiol. 1991; 261:F787–F791.
30. Dorsam J, Knopp MV, Carl S, Oesingmann N, Schad L, Brkovic D, van Kaick G, Staehler G. Ureteral complications after kidney transplantation—evaluation with functional magnetic resonance urography. Transplant Proc. 1997; 29:132–135. [PubMed: 9122928]
31. Dumoulin CL, Buonocore MH, Opsahl LR, Katzberg RW, Darrow RD, Morris TW, Batey C. Noninvasive measurement of renal hemodynamic functions using gadolinium enhanced magnetic resonance imaging. Magn Reson Med. 1994; 32:370–378. [PubMed: 7984069]
32. Dunn JF, Swartz HM. Blood oxygenation. Heterogeneity of hypoxic tissues monitored using bold MR imaging. Adv Exp Med Biol. 1997; 428:645–650. [PubMed: 9500110]
33. Edvinsson, L.; MacKenzie, ET.; McCulloch, J. Cerebral Blood Flow and Metabolism. New York: Raven; 1993.
34. Epstein FH, Agmon Y, Brezis M. Physiology of renal hypoxia. Ann NY Acad Sci. 1994; 718:72–81. [PubMed: 8185253]
35. Epstein FH, Veves A, Prasad PV. Effect of diabetes on renal medullary oxygenation during water diuresis. Diabetes Care. 2002; 25:575–578. [PubMed: 11874950]
36. Erley CM, Duda SH, Schlepckow S, Koehler J, Huppert PE, Strohmaier WL, Bohle A, Risler T, Osswald H. Adenosine antagonist theophylline prevents the reduction of glomerular filtration rate after contrast media application. Kidney Int. 1994; 45:1425–1431. [PubMed: 8072255]

37. Ersoy H, Jacobs P, Kent CK, Prince MR. Blood pool MR angiography of aortic stent-graft endoleak. Am J Roentgenol. 2004; 182:1181–1186. [PubMed: 15100115]
38. Flemming B, Seeliger E, Wronski T, Steer K, Arenz N, Persson PB. Oxygen and renal hemodynamics in the conscious rat. J Am Soc Nephrol. 2000; 11:18–24. [PubMed: 10616836]
39. Fommei E, Ghione S, Hilson AJ, Mezzasalma L, Oei HY, Piepsz A, Volterrani D. Captopril radionuclide test in renovascular hypertension: a European multicentre study. European Multicentre Study Group. Eur J Nucl Med. 1993; 20:617–623. [PubMed: 8370384]
40. Fox PT, Raichle ME, Mintun MA, Dence C. Nonoxidative glucose consumption during focal physiologic neural activity. Science. 1988; 241:462–464. [PubMed: 3260686]
41. Golman K, Ardenkjaer-Larsen JH, Petersson JS, Mansson S, Leunbach I. Molecular imaging with endogenous substances. Proc Natl Acad Sci USA. 2003; 100:10435–10439. [PubMed: 12930896]
42. Golman K, Ardenkjaer-Larsen JH, Svensson J, Axelsson O, Hansson G, Hansson L, Johannesson H, Leunbach I, Mansson S, Petersson JS, Pettersson G, Servin R, Wistrand LG. ^{13}C angiography. Acad Radiol. 2002; 9(Suppl 2):S507–S510. [PubMed: 12188323]
43. Golman K, Axelsson O, Johannesson H, Mansson S, Olofsson C, Petersson JS. Parahydrogen-induced polarization in imaging: subsecond ^{13}C angiography. Magn Reson Med. 2001; 46:1–5. [PubMed: 11443703]
44. Grenier N, Trillaud H, Combe C, Degreze P, Jeandot R, Gosse P, Douws C, Palussiere J. Diagnosis of renovascular hypertension: feasibility of captopril-sensitized dynamic MR imaging and comparison with captopril scintigraphy. Am J Roentgenol. 1996; 166:835–843. [PubMed: 8610560]
45. Gur D, Good WF, Wolfson SK Jr, Yonas H, Shabason L. In vivo mapping of local cerebral blood flow by xenon-enhanced computed tomography. Science. 1982; 215:1267–1268. [PubMed: 7058347]
46. Guyton AC, Coleman TG, Cowley AV Jr, Scheel KW, Manning RD Jr, Norman RA Jr. Arterial pressure regulation. Overriding dominance of the kidneys in long-term regulation and in hypertension. Am J Med. 1972; 52:584–594. [PubMed: 4337474]
47. Hackstein N, Heckrodt J, Rau WS. Measurement of single-kidney glomerular filtration rate using a contrast-enhanced dynamic gradient-echo sequence and the Rutland-Patlak plot technique. J Magn Reson Imaging. 2003; 18:714–725. [PubMed: 14635157]
48. Hackstein N, Kooijman H, Tomaselli S, Rau WS. Glomerular filtration rate measured using the Patlak plot technique and contrast-enhanced dynamic MRI with different amounts of gadolinium-DTPA. J Magn Reson Imaging. 2005; 22:406–414. [PubMed: 16106358]
49. Heyman SN, Fuchs S, Jaffe R, Shina A, Ellezian L, Brezis M, Rosen S. Renal microcirculation and tissue damage during acute ureteral obstruction in the rat: effect of saline infusion, indomethacin and radio-contrast. Kidney Int. 1997; 51:653–663. [PubMed: 9067896]
50. Heyman SN, Goldfarb M, Darmon D, Brezis M. Tissue oxygenation modifies nitric oxide bioavailability. Microcirculation. 1999; 6:199–203. [PubMed: 10501093]
51. Heyman SN, Kaminski N, Brezis M. Dopamine increases renal medullary blood flow without improving regional hypoxia. Exp Nephrol. 1995; 3:331–337. [PubMed: 8528677]
52. Heyman SN, Rosen S, Fuchs S, Epstein FH, Brezis M. Myoglobinuric acute renal failure in the rat: a role for medullary hypoperfusion, hypoxia, and tubular obstruction. J Am Soc Nephrol. 1996; 7:1066–1074. [PubMed: 8829123]
53. Holden C. Polygraph screening: panel seeks truth in lie detector debate. Science. 2001; 291:967. [PubMed: 11232574]
54. Huang AJ, Lee VS, Rusinek H. MR imaging of renal function. Radiol Clin North Am. 2003; 41:1001–1017. [PubMed: 14521206]
55. Johansson E, Mansson S, Wirestam R, Svensson J, Petersson JS, Golman K, Stahlberg F. Cerebral perfusion assessment by bolus tracking using hyperpolarized ^{13}C. Magn Reson Med. 2004; 51:464–472. [PubMed: 15004786]
56. Johnson RJ, Herrera-Acosta J, Schreiner GF, Rodriguez-Iturbe B. Subtle acquired renal injury as a mechanism of salt-sensitive hypertension. N Engl J Med. 2002; 346:913–923. [PubMed: 11907292]

57. Johnson RJ, Rodriguez-Iturbe B, Nakagawa T, Kang DH, Feig DI, Herrera-Acosta J. Subtle renal injury is likely a common mechanism for salt-sensitive essential hypertension. Hypertension. 2005; 45:326–330. [PubMed: 15655117]
58. Jones, RA.; Kirsch, AJ.; Grattan-Smith, JD. Estimation of GFR in the infant kidney. Proceedings of the International Society of Magnetic Resonance in Medicine; Miami. 2005; Berkeley, CA: International Society of Magnetic Resonance in Medicine; 2005. p. 553
59. Jones RA, Perez-Brayfield MR, Kirsch AJ, Grattan-Smith JD. Renal transit time with MR urography in children. Radiology. 2004; 233:41–50. [PubMed: 15317951]
60. Juillard L, Lerman LO, Kruger DG, Haas JA, Rucker BC, Polzin JA, Riederer SJ, Romero JC. Blood oxygen level-dependent measurement of acute intra-renal ischemia. Kidney Int. 2004; 65:944–950. [PubMed: 14871414]
61. Karger N, Biederer J, Lusse S, Grimm J, Steffens J, Heller M, Gluer C. Quantitation of renal perfusion using arterial spin labeling with FAIR-UFLARE. Magn Reson Imaging. 2000; 18:641–647. [PubMed: 10930773]
62. Kety S, Schmidt CF. Nitrous oxide method for the quantitative determination of cerebral blood flow in man: theory, procedure, and normal values. J Clin Invest. 1948; 27:475–483.
63. Kirchin MA, Runge VM. Contrast agents for magnetic resonance imaging: safety update. Top Magn Reson Imaging. 2003; 14:426–435. [PubMed: 14625469]
64. Langleben DD, Schroeder L, Maldjian JA, Gur RC, McDonald S, Ragland JD, O'Brien CP, Childress AR. Brain activity during simulated deception: an event-related functional magnetic resonance study. Neuroimage. 2002; 15:727–732. [PubMed: 11848716]
65. Lassen NA. Cerebral transit of an intravascular tracer may allow measurement of regional blood volume but not regional blood flow. J Cereb Blood Flow Metab. 1984; 4:633–634. [PubMed: 6501448]
66. Lassen, NA.; Perl, W. Tracer Kinetic Methods in Medical Physiology. New York: Raven; 1979.
67. Lauffer RB, Parmelee DJ, Dunham SU, Ouellet HS, Dolan RP, Witte S, McMurry TJ, Walovitch RC. MS-325: albumin-targeted contrast agent for MR angiography. Radiology. 1998; 207:529–538. [PubMed: 9577506]
68. Laurent D, Poirier K, Wasvary J, Rudin M. Effect of essential hypertension on kidney function as measured in rat by dynamic MRI. Magn Reson Med. 2002; 47:127–134. [PubMed: 11754451]
69. Le Bihan D, Breton E, Lallemand D, Aubin ML, Vignaud J, Laval-Jeantet M. Separation of diffusion and perfusion in intravoxel incoherent motion MR imaging. Radiology. 1988; 168:497–505. [PubMed: 3393671]
70. Lee, VS.; Rusinek, H.; Kim, S.; Leonard, E.; Lee, P.; Johnson, G. Analysis of dynamic three-dimensional (3D) MR renography: regional characterization by multicompartmental modeling. Proceedings of the International Society of Magnetic Resonance in Medicine; Honolulu. 2001; Berkeley, CA: International Society of Magnetic Resonance in Medicine; 2001. p. 2058
71. Li, L.; Dunkle, E.; Pierchala, L.; Prasad, P. Effect of nitric oxide inhibition on intra-renal oxygenation in humans by BOLD MRI. Proceedings of the Radiological Society of North America; Chicago. 2004; Oak Brook, IL: Radiological Society of North America; 2004. p. 384
72. Li, L.; Ji, L.; Santos, E.; Pierchala, L.; Dunkle, E.; Fogelson, L.; Prasad, P. Effect of NOS inhibition by L-NAME on intra-renal BOLD MRI: dose response in rat and human kidneys. Proceedings of the International Society of Magnetic Resonance in Medicine; Miami. 2005; Berkeley, CA: International Society of Magnetic Resonance in Medicine; 2005. p. 559
73. Li L, Li B, Storey P, Fogelson L, Li W, Prasad P. Effect of oxygen free radical scavenger (tempol) on intra-renal oxygenation in hypertensive rats as evaluated by BOLD MRI. J Magn Reson Imaging. 2005; 21:245–248. [PubMed: 15723382]
74. Li L, Storey P, Kim D, Li W, Prasad P. Kidneys in hypertensive rats show reduced response to nitric oxide synthase inhibition as evaluated by BOLD MRI. J Magn Reson Imaging. 2003; 17:671–675. [PubMed: 12766896]
75. Li LP, Storey P, Pierchala L, Li W, Polzin J, Prasad P. Evaluation of the reproducibility of intrarenal R2* and DeltaR2* measurements following administration of furosemide and during waterload. J Magn Reson Imaging. 2004; 19:610–616. [PubMed: 15112311]

76. Li W, Tutton S, Vu AT, Pierchala L, Li BS, Lewis JM, Prasad PV, Edelman RR. First-pass contrast-enhanced magnetic resonance angiography in humans using ferumoxytol, a novel ultrasmall superpara-magnetic iron oxide (USPIO)-based blood pool agent. J Magn Reson Imaging. 2005; 21:46–52. [PubMed: 15611942]
77. Liss P, Carlsson PO, Palm F, Hansell P. Adenosine A1 receptors in contrast media-induced renal dysfunction in the normal rat. Eur Radiol. 2004; 14:1297–1302. [PubMed: 14714138]
78. Liss P, Nygren A, Hansell P. Hypoperfusion in the renal outer medulla after injection of contrast media in rats. Acta Radiol. 1999; 40:521–527. [PubMed: 10485242]
79. Liu AS, Xie JX. Functional evaluation of normothermic ischemia and reperfusion injury in dog kidney by combining MR diffusion-weighted imaging and Gd-DTPA enhanced first-pass perfusion. J Magn Reson Imaging. 2003; 17:683–693. [PubMed: 12766898]
80. Lloyd D. Functional MRI and the study of human consciousness. J Cogn Neurosci. 2002; 14:818–831. [PubMed: 12191448]
81. Lo YL, Fook-Chong S, Tan EK. Increased cortical excitability in human deception. Neuroreport. 2003; 14:1021–1024. [PubMed: 12802195]
82. Louie AY, Huber MM, Ahrens ET, Rothbacher U, Moats R, Jacobs RE, Fraser SE, Meade TJ. In vivo visualization of gene expression using magnetic resonance imaging. Nat Biotechnol. 2000; 18:321–325. [PubMed: 10700150]
83. MacFall JR, Charles HC, Black RD, Middleton H, Swartz JC, Saam B, Driehuys B, Erickson C, Happer W, Cates GD, Johnson GA, Ravin CE. Human lung air spaces: potential for MR imaging with hyperpolarized He-3. Radiology. 1996; 200:553–558. [PubMed: 8685356]
84. Maril N, Margalit R, Mispelter J, Degani H. Functional sodium magnetic resonance imaging of the intact rat kidney. Kidney Int. 2004; 65:927–935. [PubMed: 14871412]
85. Martirosian P, Klose U, Mader I, Schick F. FAIR true-FISP perfusion imaging of the kidneys. Magn Reson Med. 2004; 51:353–361. [PubMed: 14755661]
86. Matthews PM, Jezzard P. Functional magnetic resonance imaging. J Neurol Neurosurg Psychiatry. 2004; 75:6–12. [PubMed: 14707297]
87. Michaely HJ, Schoenberg SO, Ittrich C, Dikow R, Bock M, Guenther M. Renal disease: value of functional magnetic resonance imaging with flow and perfusion measurements. Invest Radiol. 2004; 39:698–705. [PubMed: 15486531]
88. Mitchell DG, Tobin M, LeVeen R, Tomaczewski J, Alavi A, Staum M, Kundel H. Induced renal artery stenosis in rabbits: magnetic resonance imaging, angiography, and radionuclide determination of blood volume and blood flow. Magn Reson Imaging. 1988; 6:113–124. [PubMed: 3374282]
89. Montet X, Ivancevic MK, Belenger J, Jorge-Costa M, Pochon S, Pechere A, Terrier F, Vallee JP. Noninvasive measurement of absolute renal perfusion by contrast medium-enhanced magnetic resonance imaging. Invest Radiol. 2003; 38:584–592. [PubMed: 12960528]
90. Mori S, Eleff SM, Pilatus U, Mori N, van Zijl PC. Proton NMR spectroscopy of solvent-saturable resonances: a new approach to study pH effects in situ. Magn Reson Med. 1998; 40:36–42. [PubMed: 9660550]
91. Morishita S, Sumi M, Nishimura R, Takahashi M, Iriguchi N. Carbon-13 chemical shift imaging of [1-^{13}C]glucose under metabolism in the rat head in vivo. Radiat Med. 1992; 10:94–100. [PubMed: 1509107]
92. Mostafavi MR, Chavez DR, Cannillo J, Saltzman B, Prasad PV. Redistribution of renal blood flow after SWL evaluated by Gd-DTPA-enhanced magnetic resonance imaging. J Endourol. 1998; 12:9–12. [PubMed: 9531143]
93. Mostafavi MR, Saltzman B, Prasad PV. Magnetic resonance imaging in the evaluation of ureteropelvic junction obstructed kidney. Urology. 1997; 50:601–602. discussion 602–603. [PubMed: 9338740]
94. Muller MF, Prasad PV, Bimmler D, Kaiser A, Edelman RR. Functional imaging of the kidney by means of measurement of the apparent diffusion coefficient. Radiology. 1994; 193:711–715. [PubMed: 7972811]
95. Nagrani, NK.; Mattson, DL.; Jesmanowicz, A.; Greene, AS.; Cowley, AV., Jr; Hyde, JS. In vivo high resolution echo-planar imaging of rat kidney. Proceedings of Society of Magnetic Resonance

in Medicine; San Francisco. 1994; Berkeley, CA: Society of Magnetic Resonance in Medicine; 1994. p. 1019

96. Niendorf ER, Grist TM, Lee FT Jr, Brazy PC, Santyr GE. Rapid in vivo measurement of single-kidney extraction fraction and glomerular filtration rate with MR imaging. Radiology. 1998; 206:791–798. [PubMed: 9494503]
97. Nitz WR. Fast and ultrafast non-echo-planar MR imaging techniques. Eur Radiol. 2002; 12:2866–2882. [PubMed: 12439564]
98. Ogawa S, Lee TM, Barrere B. The sensitivity of magnetic resonance image signals of a rat brain to changes in the cerebral venous blood oxygenation. Magn Reson Med. 1993; 29:205–210. [PubMed: 8429784]
99. Ogawa S, Lee TM, Kay AR, Tank DW. Brain magnetic resonance imaging with contrast dependent on blood oxygenation. Proc Natl Acad Sci USA. 1990; 87:9868–9872. [PubMed: 2124706]
100. Ogawa S, Menon RS, Tank DW, Kim SG, Merkle H, Ellermann JM, Ugurbil K. Functional brain mapping by blood oxygenation level-dependent contrast magnetic resonance imaging. A comparison of signal characteristics with a biophysical model. Biophys J. 1993; 64:803–812. [PubMed: 8386018]
101. Padhani AR. Dynamic contrast-enhanced MRI in clinical oncology: current status and future directions. J Magn Reson Imaging. 2002; 16:407–422. [PubMed: 12353256]
102. Palm F, Bergqvist D, Carlsson PO, Hellberg O, Nyman R, Hansell P, Liss P. The effects of carbon dioxide versus ioxaglate in the rat kidney. J Vasc Interv Radiol. 2005; 16:269–274. [PubMed: 15713929]
103. Palm F, Carlsson PO, Hansell P, Hellberg O, Nygren A, Liss P. Altered response in renal blood flow and oxygen tension to contrast media in diabetic rats. Acta Radiol. 2003; 44:347–353. [PubMed: 12752011]
104. Palm F, Cederberg J, Hansell P, Liss P, Carlsson PO. Reactive oxygen species cause diabetes-induced decrease in renal oxygen tension. Diabetologia. 2003; 46:1153–1160. [PubMed: 12879251]
105. Palm F, Hansell P, Ronquist G, Waldenstrom A, Liss P, Carlsson PO. Polyol-pathway-dependent disturbances in renal medullary metabolism in experimental insulin-deficient diabetes mellitus in rats. Diabetologia. 2004; 47:1223–1231. [PubMed: 15232683]
106. Palm F, Ortsater H, Hansell P, Liss P, Carlsson PO. Differentiating between effects of streptozotocin per se and subsequent hyperglycemia on renal function and metabolism in the streptozotocin-diabetic rat model. Diabetes Metab Res Rev. 2004; 20:452–459. [PubMed: 15386825]
107. Pedersen M, Dissing TH, Morkenborg J, Stodkilde-Jorgensen H, Hansen LH, Pedersen LB, Grenier N, Frøkiær J. Validation of quantitative BOLD MRI measurements in kidney: application to unilateral ureteral obstruction. Kidney Int. 2005; 67:2305–2312. [PubMed: 15882272]
108. Pennell DJ. Cardiovascular magnetic resonance and the role of adenosine pharmacologic stress. Am J Cardiol. 2004; 94:26D–32D.
109. Perman WH, Gado MH, Larson KB, Perlmutter JS. Simultaneous MR acquisition of arterial and brain signal-time curves. Magn Reson Med. 1992; 28:74–83. [PubMed: 1435223]
110. Prasad PV, Cannillo J, Chavez DR, Pinchasin ES, Dolan RP, Walovitch R, Edelman RR. First-pass renal perfusion imaging using MS-325, an albumin-targeted MRI contrast agent. Invest Radiol. 1999; 34:566–571. [PubMed: 10485071]
111. Prasad PV, Chen Q, Goldfarb JW, Epstein FH, Edelman RR. Breath-hold R2* mapping with a multiple gradient-recalled echo sequence: application to the evaluation of intrarenal oxygenation. J Magn Reson Imaging. 1997; 7:1163–1165. [PubMed: 9400864]
112. Prasad PV, Edelman RR, Epstein FH. Noninvasive evaluation of intrarenal oxygenation with BOLD MRI. Circulation. 1996; 94:3271–3275. [PubMed: 8989140]
113. Prasad PV, Epstein FH. Changes in renal medullary P_{O_2} during water diuresis as evaluated by blood oxygenation level-dependent magnetic resonance imaging: effects of aging and cyclooxygenase inhibition. Kidney Int. 1999; 55:294–298. [PubMed: 9893139]

114. Prasad PV, Goldfarb J, Sundaram C, Priatna A, Li W, Edelman RR. Captopril MR renography in a swine model: toward a comprehensive evaluation of renal arterial stenosis. Radiology. 2000; 217:813–818. [PubMed: 11110948]
115. Prasad PV, Kim D, Kaiser AM, Chavez D, Gladstone S, Li W, Buxton RB, Edelman RR. Noninvasive comprehensive characterization of renal artery stenosis by combination of STAR angiography and EPISTAR perfusion imaging. Magn Reson Med. 1997; 38:776–787. [PubMed: 9358452]
116. Prasad PV, Priatna A, Spokes K, Epstein FH. Changes in intrarenal oxygenation as evaluated by BOLD MRI in a rat kidney model for radiocontrast nephropathy. J Magn Reson Imaging. 2001; 13:744–747. [PubMed: 11329196]
117. Priatna A, Epstein FH, Spokes K, Prasad PV. Evaluation of changes in intrarenal oxygenation in rats using multiple gradient-recalled echo (mGRE) sequence. J Magn Reson Imaging. 1999; 9:842–846. [PubMed: 10373033]
118. Radermacher J, Chavan A, Bleck J, Vitzthum A, Stoess B, Gebel MJ, Galanski M, Koch KM, Haller H. Use of Doppler ultrasonography to predict the outcome of therapy for renal-artery stenosis. N Engl J Med. 2001; 344:410–417. [PubMed: 11172177]
119. Raghunand N, Howison C, Sherry AD, Zhang S, Gillies RJ. Renal and systemic pH imaging by contrast-enhanced MRI. Magn Reson Med. 2003; 49:249–257. [PubMed: 12541244]
120. Rajagopalan P, Krishnan KR, Passe TJ, Macfall JR. Magnetic resonance imaging using deoxyhemoglobin contrast versus positron emission tomography in the assessment of brain function. Prog Neuropsychopharmacol Biol Psychiatry. 1995; 19:351–366. [PubMed: 7624487]
121. Ries M, Basseau F, Tyndal B, Jones R, Deminiere C, Catargi B, Combe C, Moonen CW, Grenier N. Renal diffusion and BOLD MRI in experimental diabetic nephropathy. Blood oxygen level-dependent. J Magn Reson Imaging. 2003; 17:104–113. [PubMed: 12500279]
122. Ries M, Jones RA, Basseau F, Moonen CT, Grenier N. Diffusion tensor MRI of the human kidney. J Magn Reson Imaging. 2001; 14:42–49. [PubMed: 11436213]
123. Rohrschneider WK, Becker K, Hoffend J, Clorius JH, Darge K, Kooijman H, Troger J. Combined static-dynamic MR urography for the simultaneous evaluation of morphology and function in urinary tract obstruction. II. Findings in experimentally induced ureteric stenosis. Pediatr Radiol. 2000; 30:523–532. [PubMed: 10993536]
124. Rohrschneider WK, Hoffend J, Becker K, Clorius JH, Darge K, Kooijman H, Troger J. Combined static-dynamic MR urography for the simultaneous evaluation of morphology and function in urinary tract obstruction. I. Evaluation of the normal status in an animal model. Pediatr Radiol. 2000; 30:511–522. [PubMed: 10993535]
125. Roman RJ, Carmines PK, Loutzenhiser R, Conger JD. Direct studies on the control of the renal microcirculation. J Am Soc Nephrol. 1991; 2:136–149. [PubMed: 1954326]
126. Roman RJ, Zou AP. Influence of the renal medullary circulation on the control of sodium excretion. Am J Physiol Regul Integr Comp Physiol. 1993; 265:R963–R973.
127. Rosen S, Epstein FH, Brezis M. Determinants of intrarenal oxygenation: factors in acute renal failure. Ren Fail. 1992; 14:321–325. [PubMed: 1509164]
128. Sadowski EA, Fain SB, Alford SK, Korosec FR, Fine J, Meuhrer R, Djamali A, Hofmann RM, Becker BN, Grist TM. Assessment of acute renal transplant rejection with blood oxygen level-dependent MR imaging: initial experience. Radiology. 2005; 236:911–919. [PubMed: 16118170]
129. Salerno M, Altes TA, Mugler JP, Nakatsu M 3rd, Hatabu H, de Lange EE. Hyperpolarized noble gas MR imaging of the lung: potential clinical applications. Eur J Radiol. 2001; 40:33–44. [PubMed: 11673006]
130. Salerno M, de Lange EE, Altes TA, Truwit JD, Brookeman JR, Mugler JP III. Emphysema: hyperpolarized helium 3 diffusion MR imaging of the lungs compared with spirometric indexes–initial experience. Radiology. 2002; 222:252–260. [PubMed: 11756734]
131. Schmieder AH, Winter PM, Caruthers SD, Harris TD, Williams TA, Allen JS, Lacy EK, Zhang H, Scott MJ, Hu G, Robertson JD, Wickline SA, Lanza GM. Molecular MR imaging of melanoma angiogenesis with $\alpha v\beta_3$-targeted paramagnetic nanoparticles. Magn Reson Med. 2005; 53:621–627. [PubMed: 15723405]

132. Schoenberg SO, Aumann S, Just A, Bock M, Knopp MV, Johansson LO, Ahlstrom H. Quantification of renal perfusion abnormalities using an intravascular contrast agent (part 2): results in animals and humans with renal artery stenosis. Magn Reson Med. 2003; 49:288–298. [PubMed: 12541249]
133. Schoenberg SO, Just A, Bock M, Knopp MV, Persson PB, Kirchheim HR. Noninvasive analysis of renal artery blood flow dynamics with MR cine phase-contrast flow measurements. Am J Physiol Heart Circ Physiol. 1997; 272:H2477–H2484.
134. Schoenberg SO, Knopp MV, Londy F, Krishnan S, Zuna I, Lang N, Essig M, Hawighorst H, Maki JH, Stafford-Johnson D, Kallinowski F, Chenevert TL, Prince MR. Morphologic and functional magnetic resonance imaging of renal artery stenosis: a multireader tricenter study. J Am Soc Nephrol. 2002; 13:158–169. [PubMed: 11752033]
135. Siegel CL, Aisen AM, Ellis JH, Londy F, Chenevert TL. Feasibility of MR diffusion studies in the kidney. J Magn Reson Imaging. 1995; 5:617–620. [PubMed: 8574050]
136. Smith, AM.; Materne, R.; Van Beers, BE. Quantitative measurement of blood perfusion, GFR and arterial vascular fraction in the kidney cortex. Proceedings of International Society of Magnetic Resonance in Medicine; Honolulu. 2001; Berkeley, CA: International Society of Magnetic Resonance in Medicine; 2001. p. 367
137. Solomon R, Werner C, Mann D, D'Elia J, Silva P. Effects of saline, mannitol, and furosemide to prevent acute decreases in renal function induced by radiocontrast agents. N Engl J Med. 1994; 331:1416–1420. [PubMed: 7969280]
138. Stewart GN. Researches on the circulation time in organs, and on the influences which affect it: parts I–III. J Physiol. 1894; 15:1–89.
139. Stiles J, Moses P, Passarotti A, Dick FK, Buxton R. Exploring developmental change in the neural bases of higher cognitive functions: the promise of functional magnetic resonance imaging. Dev Neuropsychol. 2003; 24:641–668. [PubMed: 14561565]
140. Storey, P. Introduction to magnetic resonance imaging and spectroscopy. In: Prasad, P., editor. Magnetic Resonance Imaging: Methods and Biological Applications. Totowa, NJ: Humana; 2005. p. 3-58.
141. Strohmaier WL, Bichler KH, Koch J, Balk N, Wilbert DM. Protective effect of verapamil on shock wave induced renal tubular dysfunction. J Urol. 1993; 150:27–29. [PubMed: 7685425]
142. Stubbs M, Bhujwalla ZM, Tozer GM, Rodrigues LM, Maxwell RJ, Morgan R, Howe FA, Griffiths JR. An assessment of 31P MRS as a method of measuring pH in rat tumours. NMR Biomed. 1992; 5:351–359. [PubMed: 1489671]
143. Svensson J, Mansson S, Johansson E, Petersson JS, Olsson LE. Hyperpolarized ^{13}C MR angiography using trueFISP. Magn Reson Med. 2003; 50:256–262. [PubMed: 12876701]
144. Taylor A. Functional testing: ACEI renography. Semin Nephrol. 2000; 20:437–444. [PubMed: 11022896]
145. Teh HS, Ang ES, Wong WC, Tan SB, Tan AG, Chng SM, Lin MB, Goh JS. MR renography using a dynamic gradient-echo sequence and low-dose gadopentetate dimeglumine as an alternative to radionuclide renography. Am J Roentgenol. 2003; 181:441–450. [PubMed: 12876024]
146. Trueta, J.; Barclay, AF.; Daniel, PM.; Franklin, KJ.; Prichard, MML. Studies of the Renal Circulation. Oxford, UK: Blackwell; 1947.
147. Ugurbil K, Hu X, Chen W, Zhu XH, Kim SG, Georgopoulos A. Functional mapping in the human brain using high magnetic fields. Philos Trans R Soc Lond B Biol Sci. 1999; 354:1195–1213. [PubMed: 10466146]
148. Vallee JP, Lazeyras F, Khan HG, Terrier F. Absolute renal blood flow quantification by dynamic MRI and Gd-DTPA. Eur Radiol. 2000; 10:1245–1252. [PubMed: 10939483]
149. Van Sluis R, Bhujwalla ZM, Raghunand N, Ballesteros P, Alvarez J, Cerdan S, Galons JP, Gillies RJ. In vivo imaging of extracellular pH using ^{1}H MRSI. Magn Reson Med. 1999; 41:743–750. [PubMed: 10332850]
150. Wang JJ, Hendrich KS, Jackson EK, Ildstad ST, Williams DS, Ho C. Perfusion quantitation in transplanted rat kidney by MRI with arterial spin labeling. Kidney Int. 1998; 53:1783–1791. [PubMed: 9607213]

151. Weisskoff RM, Chesler D, Boxerman JL, Rosen BR. Pitfalls in MR measurement of tissue blood flow with intravascular tracers: which mean transit time? Magn Reson Med. 1993; 29:553–558. [PubMed: 8464373]

152. Young IR, Hall AS, Bryant DJ, Thomas DG, Gill SS, Dubowitz LM, Cowan F, Pennock JM, Bydder GM. Assessment of brain perfusion with MR imaging. J Comput Assist Tomogr. 1988; 12:721–727. [PubMed: 3170829]

153. Zeirler KL. Theoretical basis of indicator-dilution methods for measuring flow and volume. Circ Res. 1962; 10:393–407.

154. Zhang W, Williams DS, Detre JA, Koretsky AP. Measurement of brain perfusion by volume-localized NMR spectroscopy using inversion of arterial water spins: accounting for transit time and cross-relaxation. Magn Reson Med. 1992; 25:362–371. [PubMed: 1614321]

155. Zoula, S.; Hofmann, L.; Giger, A.; Vogt, B.; Vock, P.; Frey, F.; Boesch, C. Quantification of renal R2* index using BOLD MRI: reproducibility and observation of age-dependence. Proceedings of International Society of Magnetic Resonance in Medicine; Kyoto. 2004; Berkeley, CA: International Society of Magnetic Resonance in Medicine; p. 563

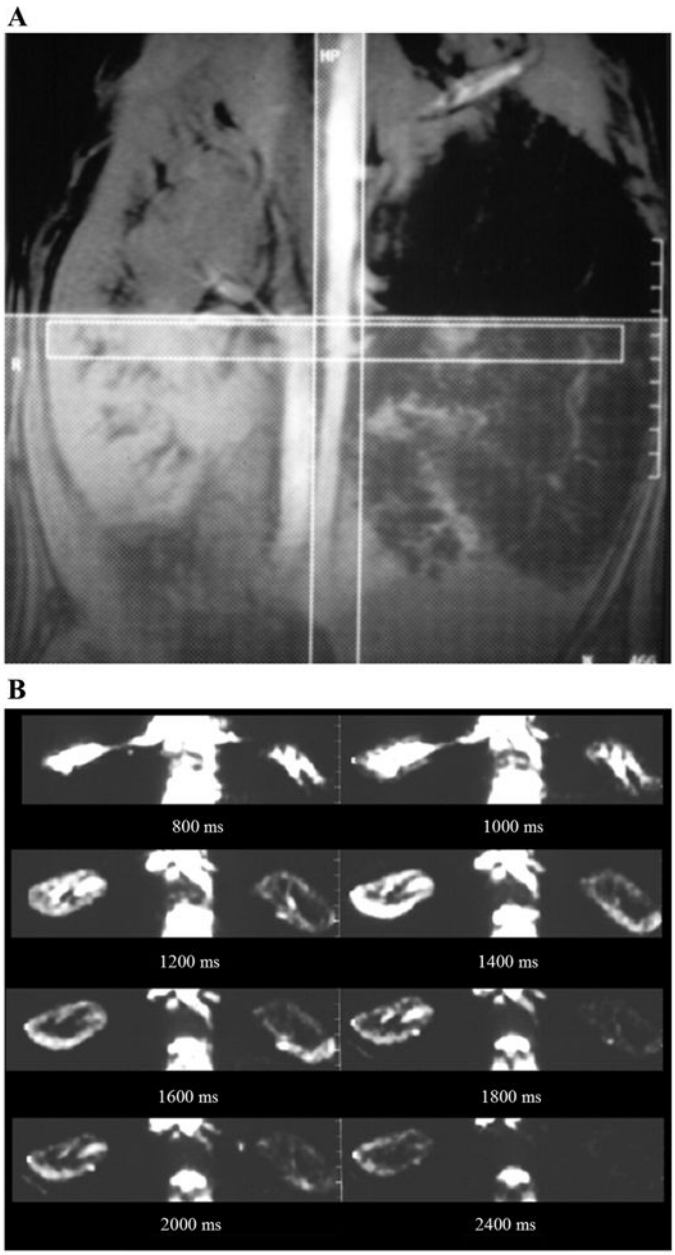

Fig. 1.

Renal perfusion magnetic resonance imagery (MRI) by arterial spin labeling (ASL). *A*: method of acquiring MRI following ASL. The vertical stripe illustrates the labeling radio frequency (RF) pulse applied so that all the spins in the descending aorta are inverted. The horizontal stripe is a representation of the transverse slice of interest through the kidneys. The thick hatched slab (*right*) represents a presaturation pulse applied to avoid any venous contribution to the observed signal intensity and to minimize any artifacts due to peristaltic motion in the abdomen. Two acquisitions were performed, one with and one without the labeling pulse. The difference image would then be a representation of all the labeled blood that enters the slice of interest. Obviously, this varies as a function of time delay between the labeling pulse and the acquisition. *B*: set of transverse (difference) images through the kidneys obtained after different delay times in a swine model with a chronic renal artery

stenosis in the left kidney (*right*). Based on this set of data, it is possible to estimate absolute perfusion (115).

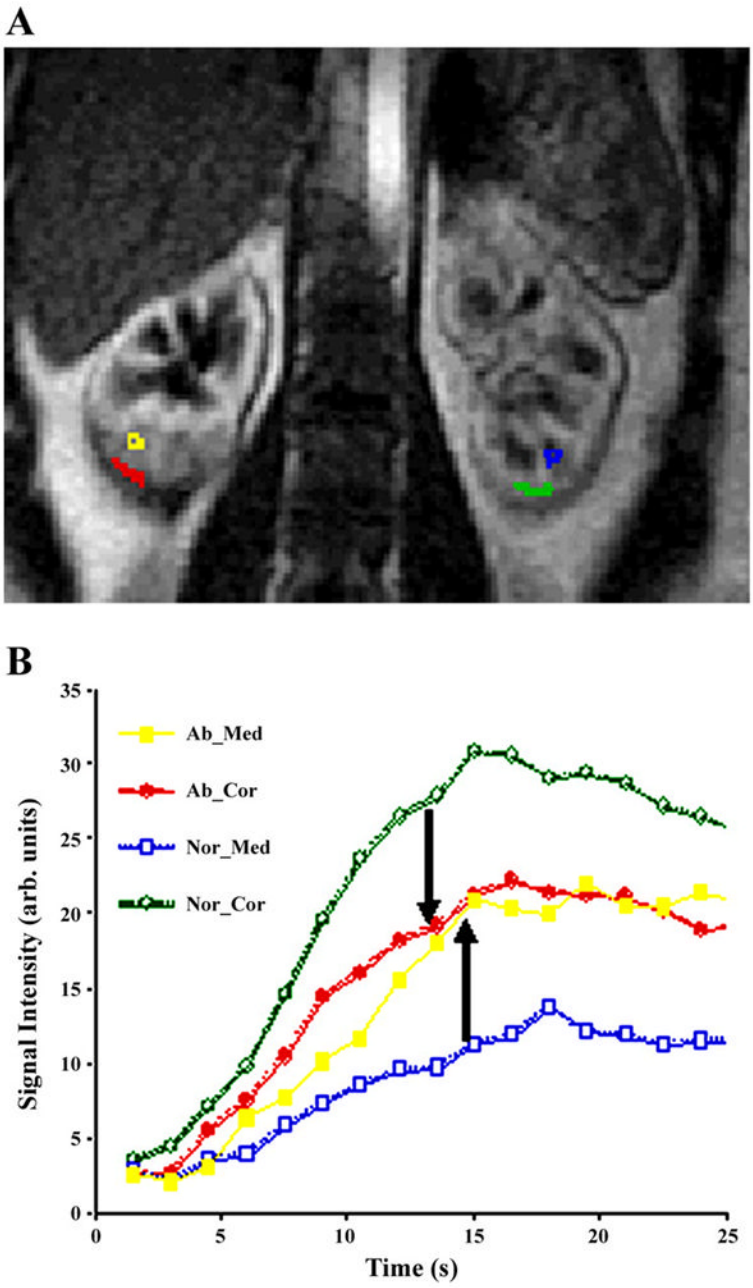

Fig. 2.

Gadolinium (Gd)-diethylenetriamine pentaacetic acid (DTPA)-enhanced first-pass perfusion imaging in a human subject following extracorporeal shock wave lithotripsy (ESWL). Shown is a representative perfusion image (*A*) along with the regions of interest used for signal intensity vs. time plots (*B*). The blurring of corticomedullary differentiation in the lower pole of the right kidney indicates where the ESWL was focused. Note that the cortical curve in the affected region (Ab Cor) is lower than normal (Nor Cor), whereas the medullary curve in the affected region (Ab Med) is higher than normal (Nor Med). With the use of the slope of these curves as a relative perfusion index, it was shown that there is a reduction in cortical flow (~30%) with a concomitant increase in the medullary flow (34 ± 14%) in the region where ESWL in focused. Reprinted from Ref. 94 with permission.

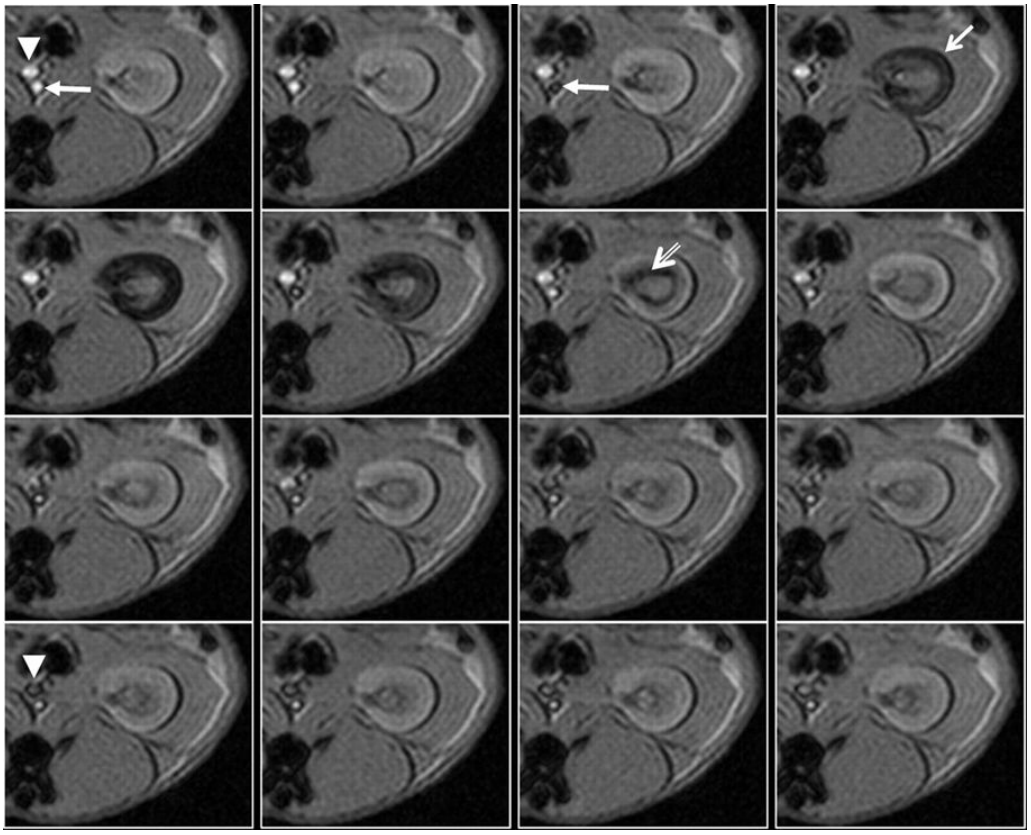

Fig. 3.

Use of intravascular contrast agents for perfusion MRI. Shown is a representative series of kidney images in a rabbit obtained using gradient echo sequence (TR/TE/FA = 15/3 ms/10^0) with a temporal resolution of 2 s (*right* to *left* and *top* to *bottom*). Ferumoxytol at a dose of 1 mg/kg was administered as a bolus through an ear vein, and the acquisition of MRI was simultaneously initiated. Marked in the 1st time frame (precontrast) are the abdominal aorta (solid arrow) and vena cava (solid arrowhead), respectively. Note in the 3rd time frame that the aorta goes completely dark. In the next time frame, the cortex gets dark (arrow), and by the 7th time frame the medulla goes completely dark whereas cortex recovers, and by the 13th time frame the vena cava becomes dark. Based on this type of dynamic scanning, one can obtain concentration vs. time profiles and fit them to appropriate mathematical models to extract various perfusion indexes (140).

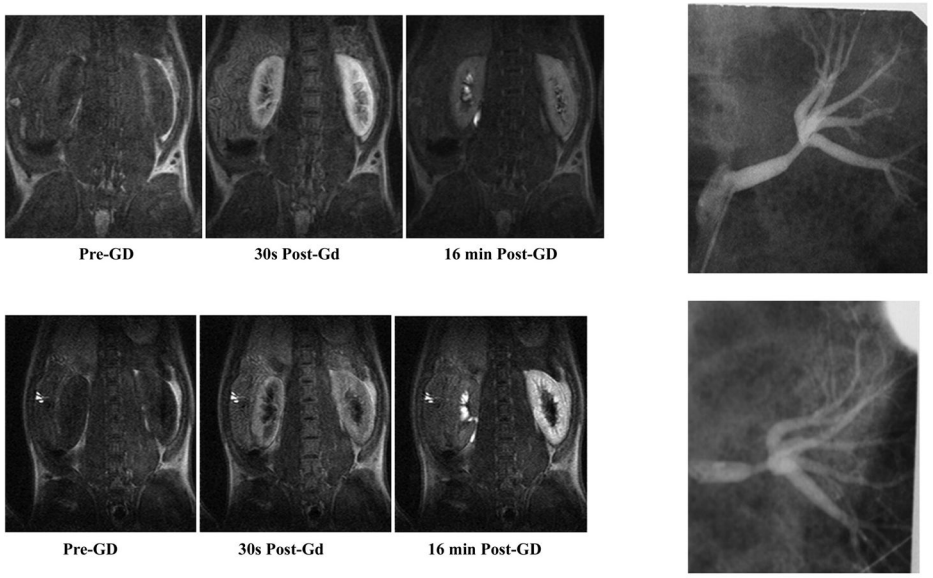

Fig. 4.

Illustration of renal function as evaluated by dynamic MRI following administration of Gd-DTPA, a positive contrast agent (i.e., with higher concentrations, the signal is increased). Shown are longitudinal relaxation (T_1)-weighted MR images obtained in a chronic renal artery stenosis model in swine at representative time points following Gd-DTPA (0.05 mmol/kg) and following administration of captopril (118). The *top* row was obtained 1 wk postsurgical placement of an MRI-compatible ameroid constrictor around the renal artery (seen on the X-ray angiograms on the *right*). The *bottom* row was obtained in the same animal 5 wk later. Note the severity of the renal artery stenosis, especially the poststenotic vessel dilatation, a classic sign of hemodynamically significant stenosis. Whereas at *week 1*, the contrast washout is almost complete and symmetrical, at *week 6*, with the progression of stenosis to a point of being hemodynamically significant, the washout in the affected kidney is rather limited. Figure reproduced from Ref. 117 with permission from *RSNA*.

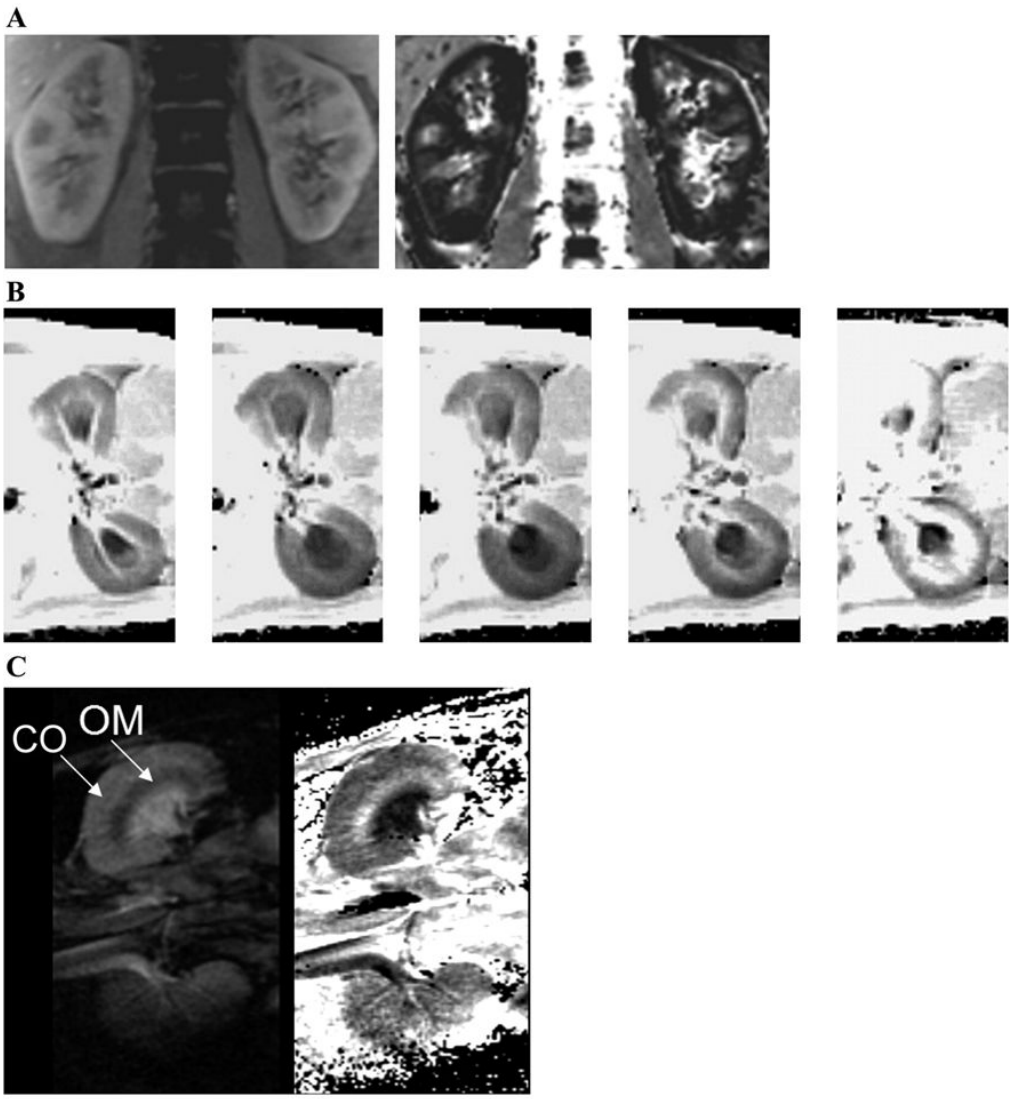

Fig. 5.

A: blood oxygenation level-dependent (BOLD) MRI data in human kidney. Shown are data acquired with a 3D sequence where the entire kidney in the coronal plane can be covered within a single breath-hold interval. Shown are images from 1 representative slice (of 6 acquired). *Left*: first image of 8 echo images acquired. *Right*: corresponding calculated rate of spin dephasing (R_2*)map. The corticomedullary differentiation on both the anatomic image and R_2* map are remarkable. The medulla appears darker on the T_1-weighted anatomic images, whereas on the R_2* maps it appears bright (signifying relatively low regional blood and hence tissue P_{O_2}). *B*: set of pre- and postpharmaceutical R_2* maps in rat kidneys in the axial plane (500-μm in-plane and 3-mm slice thickness). While this was not performed to address any specific scientific question, it is a very nice demonstration of the advantage and efficacy of the technique. These images were all acquired within ~1 h, with about 10 min between administration of different agents. Furosemide stops the reabsorptive function along the medullary thick ascending limbs and thereby reduces the oxygen consumption in the medullary segments. Thus one can observe a reduction in the brightness of R_2* maps in the medulla (lower R_2* implies better oxygenation). ANG II is a vasoconstrictor that is commonly used, and we observed little effect on the R_2* maps.

However, following subsequent administration of *N* $^{\omega}$-nitro-L-arginine methyl ester (L-NAME) and norepinephrine (potent vasoconstrictors), there was a significant increase in R_2*, predominantly in the renal medulla. *C*: BOLD MRI data in a mouse kidney. Shown are data acquired in a 24-g mouse using a dedicated 2-cm surface coil on a standard 3.0-T whole body scanner (same as for *A* and *B*). This figure provides clear indication of the power of the technology in terms of its scaling and how observations could be translated from a mouse models to humans very easily. Shown are 1 representative image (*left*; of 6 individual echo images) obtained in the coronal plane (160-μm in-plane and 500-μm slice thickness) and the calculated R_2* map (*right*). CO, cortex; OM, outer medulla.

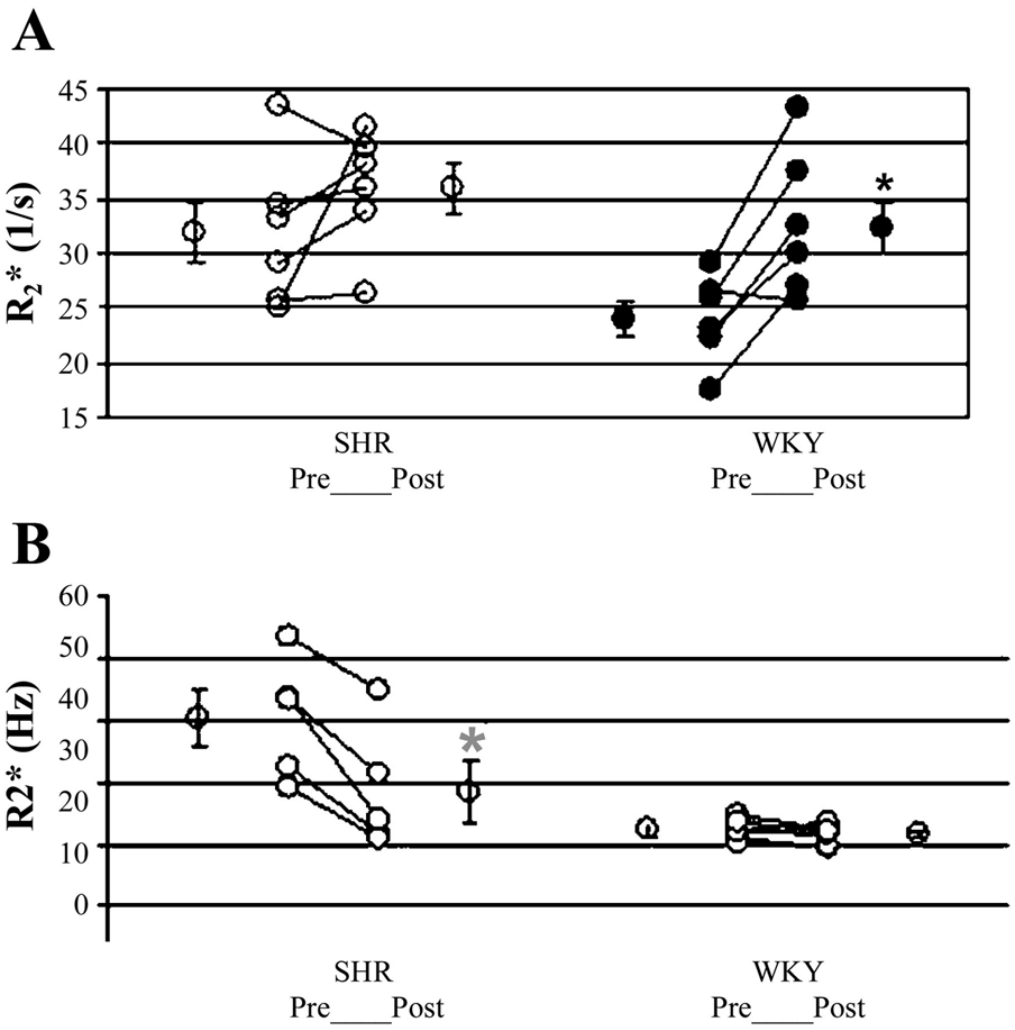

Fig. 6.

A: illustration of individual changes post-L-NAME in spontaneously hypertensive (SHR) and Wistar-Kyoto (WKY) rats. The average (means ± SE) of all points acquired at least 20 min after L-NAME administration was used as postmaneuver R_2*. Mean R_2* values pre- and post-L-NAME in the renal medulla were averaged over all rats of each strain. WKY rats showed significant response to L-NAME in the medulla, as evaluated by BOLD MRI measurements. SHRs did not show significant response to L-NAME. Also, note that the pre-L-NAME, R_2* in SHRs is similar in magnitude to post-L-NAME in WKY. Figure reproduced from Ref. 75 with permission from Wiley InterScience. *B*: illustration of individual changes posttempol in SHR and WKY rats. Average (means ± SE) of all points acquired at least 20 min after tempol administration was used as postmaneuver R_2*. Mean R_2* values pre- and posttempol in the renal medulla were averaged over all rats of each strain. SHR showed significant response to tempol in medulla, as evaluated by BOLD MRI measurements. WKY rats did not show significant response to tempol. Figure reproduced from Ref. 74 with permission from Wiley InterScience.